

See discussions, stats, and author profiles for this publication at: <https://www.researchgate.net/publication/236219999>

Computational Study of the Hydrolysis Reactions of Small MO₂ (M= Zr and Hf) Nanoclusters with Water

ARTICLE in THE JOURNAL OF PHYSICAL CHEMISTRY C · APRIL 2012

Impact Factor: 4.77 · DOI: 10.1021/jp210867w

CITATIONS

13

READS

32

7 AUTHORS, INCLUDING:



Zongtang Fang

University of Alabama

15 PUBLICATIONS 86 CITATIONS

[SEE PROFILE](#)



Matthew D. Outlaw

University of Alabama

1 PUBLICATION 13 CITATIONS

[SEE PROFILE](#)



David A Dixon

University of Alabama

767 PUBLICATIONS 22,217 CITATIONS

[SEE PROFILE](#)



James L Gole

Georgia Institute of Technology

356 PUBLICATIONS 7,014 CITATIONS

[SEE PROFILE](#)

Computational Study of the Hydrolysis Reactions of Small MO_2 ($\text{M} = \text{Zr}$ and Hf) Nanoclusters with Water

Zongtang Fang, Matthew D. Outlaw, Kyle K. Smith, Natalie W. Gist, Shenggang Li, and David A. Dixon*

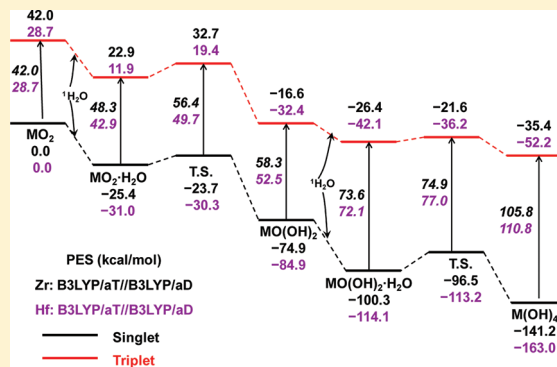
Department of Chemistry, The University of Alabama, Shelby Hall, Box 870336, Tuscaloosa, Alabama 35487-0336, United States

James L. Gole

Schools of Physics and Mechanical Engineering, Georgia Institute of Technology, Atlanta, Georgia 30332-0430, United States

Supporting Information

ABSTRACT: Density functional theory (DFT) has been used to study the hydrolysis reaction of $(\text{MO}_2)_n$ ($\text{M} = \text{Zr}, \text{Hf}$, $n = 1–4$) nanoclusters in the ground singlet and first triplet states. The reactions for singlet $n = 1$ were benchmarked at the CCSD(T) level of theory. The reactions of H_2O with the metal site having an $\text{M}=\text{O}$ bond and/or $\text{M}-\text{O}$ bonds as well as H transfer to both terminal $=\text{O}$ atoms and bridge $-\text{O}$ atoms have been studied. The partial charge on M increases as the $\text{M}=\text{O}$ bonds are replaced with $\text{M}-\text{OH}$ bonds. The first H_2O adsorption (physisorption) energies for these MO_2 nanoclusters are calculated to be -20 to -30 kcal/mol for the singlet state and -15 to -48 kcal/mol for the triplet state. These physisorption energies depend on the cluster size and the adsorption site, consistent with existing experimental and computational studies. The first hydrolysis (dissociative chemisorption) reaction energies of the MO_2 nanoclusters are calculated to have a much broader range, -30 to -80 kcal/mol for the singlet states and -30 to -100 kcal/mol for the triplet states. Steric effects play an important role in determining the physisorption and chemisorption energies, especially for the trimers and tetramers. The potential energy surfaces for hydrolysis in both the singlet and triplet states are calculated. The calculated Lewis acidities (fluoride affinities) correlate with the hydrolysis properties of the nanoclusters. Our calculations show that H_2O readily reacts with both the singlet and triplet states of the MO_2 nanoclusters to form the hydroxides. The reaction barriers are generally less than 10 kcal/mol for the singlet states, and because the H_2O physisorption energies are large, the barriers occur below the $(\text{MO}_2)_n$ asymptote.



INTRODUCTION

The Group 4 transition metal dioxide, TiO_2 , has been widely studied for hydrogen production from water under UV irradiation since the first observation of its photocatalytic activity.^{1,2} The other two Group 4 transition metal dioxides, zirconia (ZrO_2) and hafnia (HfO_2), also show photocatalytic capability^{3–6} for water splitting to generate H_2 and O_2 . With pure ZrO_2 powder, the photocatalytic decomposition of water was first observed by Sayama and Arakawa³ under UV irradiation. Cu and RuO_2 loaded ZrO_2 catalysts were found to be more efficient than the pure ZrO_2 catalyst for water decomposition, and in aqueous solution, the addition of carbonate also increased the gas evolution rate.⁴ In Na_2CO_3 solution, H_2 production has been observed with Pt and RuO_2 doped HfO_2 semiconductor catalysts.⁵ ZrO_2 was found to be more efficient than HfO_2 for hydrogen production. In addition, ZrO_2 and HfO_2 have been used as either the catalyst or the support for photocatalytic degradation of organic pollutants in wastewater.^{7,8} The mechanisms for the interaction between water and these catalysts are an important issue in photocatalysis research.

For bulk samples, both ZrO_2 and HfO_2 have three polymorphs, monoclinic, tetragonal, and cubic. ZrO_2 and HfO_2 have similar physical and chemical properties. At room temperature, the most stable phase is the monoclinic one. As the temperature increases, ZrO_2 and HfO_2 undergo phase transformations first to the tetragonal and then to the cubic.⁹ High-temperature phases, which are more technically important than the monoclinic phase, can be stabilized at room temperature by doping with cations or controlling the size of the nanoparticle.¹⁰ Nanocrystalline zirconia, synthesized at room temperature, has been reported to be tetragonal.¹¹ The bulk band gaps are dependent on the phase and are estimated to be ~ 5.8 eV for ZrO_2 and ~ 5.9 eV for HfO_2 .¹² Because these energies are much larger than the band gap of bulk TiO_2 , 3.0–3.2 eV, ZrO_2 and HfO_2 are expected to be much less efficient as photocatalysts in terms of utilizing solar radiation.

Received: November 11, 2011

Revised: March 21, 2012

Published: March 21, 2012

The interactions between bulk MO_2 ($\text{M} = \text{Zr}, \text{Hf}$) and water have been widely studied experimentally. Holmes and co-workers¹³ studied heats of immersion in the zirconium oxide–water system. The interaction of water vapor with the monoclinic and tetragonal phases of ZrO_2 was investigated, and the heats of adsorption were reported to be above -30 kcal/mol. The adsorption–desorption of submonolayer water coverage on two different zirconia phases was studied with infrared spectroscopy.¹⁴ Two high-frequency bands at 3760 and 3660 cm^{-1} were observed and assigned to chemisorbed OH groups. Ushakov and Navrotksy¹⁵ measured the heats of gas–solid interaction in the system of half-monolayer water adsorption on hafnia and zirconia. On differently prepared monoclinic HfO_2 and ZrO_2 surfaces, the adsorption enthalpies were found to be between -31 to -45 kcal/mol and -26 to -41 kcal/mol, respectively. The adsorption enthalpies on the tetragonal surfaces were much smaller, -17 kcal/mol for HfO_2 and -22 kcal/mol for ZrO_2 . The adsorption of water on Y_2O_3 -doped ZrO_2 powder has been studied by Riess.¹⁶ Water first formed a chemisorption layer followed by physisorption of a second water layer on the first chemisorbed water layer. Thermogravimetric measurements were carried out to obtain the adsorption energies. The chemisorption energies derived using a two-site Langumir model are -22.4 and -16.8 kcal/mol on two different adsorption sites. The physisorption energy, -11.4 kcal/mol, was obtained from a BET fit.¹⁷

A computational study of water interactions with the (110) and (101) tetragonal zirconia surfaces has been done using the ONIOM2 approach with B3LYP/3-21G(d) for the high-level calculations and the UFF force field for the low-level calculations.¹⁸ It was reported that water dissociated on the (101) zirconia surface producing two hydroxyl groups, and the adsorption processes were calculated to be exothermic, -51.0 kcal/mol. On the (110) surface, the dissociative chemisorption energy for H_2O was calculated to be -28.4 kcal/mol. The hydroxylated tetragonal $\text{ZrO}_2(101)$ surface has been studied by periodic density functional theory (DFT) methods.¹⁹ The calculated physisorption energy is -13.4 kcal/mol at 298 K, and the energy for the desorption of chemisorbed water was predicted to be -36.0 kcal/mol at 698 K. The adsorption of water on the monoclinic zirconia ($\bar{1}11$), ($\bar{1}01$), and (111) surfaces was also studied using DFT with the PW91 and PBE functionals.²⁰ At low water coverage (less than 25%), water was dissociated on all three stable surfaces. At high coverage, physisorption and chemisorption coexisted on different sites of the same surface. The dissociative chemisorption energies were reported to be in the range -30 to -45 kcal/mol. The average adsorption energy (from the physisorbed and chemisorbed sites on the same surface) was in the range -25 to -40 kcal/mol. Hydroxylation of both zirconia and hafnia surfaces was also studied with periodic plane-wave (PW) pseudopotential (PP) DFT.²¹ Water adsorption energies on the tetragonal zirconia (t-ZrO_2) (001) and (101) surfaces and on the (001) surface of monoclinic zirconia (m-ZrO_2) and hafnia (m-HfO_2) were calculated. Both the dissociative chemisorption and physisorption energies are dependent on the coverage and the surface plane. For zirconia, the physisorption energies were calculated to be between -7 and -24 kcal/mol, and the chemisorption energies were in the range -22 to -41 kcal/mol dependent on the coverage. For hafnia, the physisorption and chemisorption energies were calculated to be roughly -24 and -36 kcal/mol with water coverage of 50%. On the (001) surface of m-ZrO_2 (m-HfO_2), an oxygen atom adsorbs between the shortest M–

M distance and forms two M–O bonds with distances of 2.17 (2.12) and 2.29 (2.28) Å, respectively. For the t-ZrO_2 (001) surface, the M–O bond distance is 2.27 Å. Although the interaction between water and zirconia has been widely studied, the actual mechanism is still not well established. There are fewer studies of water interacting with hafnia.

We recently reported studies of the Group 4 transitional metal oxide clusters, M_nO_{2n} ($\text{M} = \text{Zr}, \text{Hf}, n = 1\text{--}4$),²² at the DFT and coupled cluster [CCSD(T)] levels to calculate their structures, heats of formation, electron attachment energies, and electron excitation energies. We found multiple low-lying structures for $n > 1$. The ground state of M_2O_4 was calculated to be ${}^1\text{A}_g$ (C_{2v} , **2a**), with two low-energy isomers of ${}^1\text{A}_1$ (C_{2v} , **2h**) and ${}^1\text{A}_1$ (C_{3v} , **2k**) symmetry. The ground state of M_3O_6 was calculated to be ${}^1\text{A}'$ (C_s , **3a**), with three low-energy isomers of ${}^1\text{A}$ (C_2 , **4a**), ${}^1\text{A}$ (C_1 , **5a**), and ${}^1\text{A}'$ (C_s , **6a**) symmetry. The ground state of M_4O_8 was calculated to be ${}^1\text{A}_1$ (C_{2v} , **7a**) with two low-energy ${}^1\text{A}_g$ (C_{2h} , **8a**) and ${}^1\text{A}_1$ (C_{2v} , **9a**) isomers. (The labeling corresponds to that in the figures discussed below.) In contrast to the bulk band gaps discussed above, the singlet–triplet energy gap for the TiO_2 nanoclusters was calculated to be 2.24 eV at the CCSD(T)/aD//B3LYP/aD level for the monomer, 2–3 eV for the dimers, 2.5–3 eV for the trimers, and 2–3.5 eV for the tetramers.²³ For $\text{M} = \text{Zr}$, the singlet–triplet energy gap was calculated to be 2 eV for the monomer, 3.0–3.5 eV for the dimers, 2.0–3.3 eV for the trimers, and 2.0–3.9 eV for the tetramers. For $\text{M} = \text{Hf}$, the singlet–triplet energy gap was calculated to be 1.5 eV for the monomer, 2.1–3.2 for the dimers, 1.6–3.1 eV for the trimers, and 1.6–3.6 eV for the tetramers.^{22b} Virtually all of the isomers of these nanoclusters have the energy gaps in the visible range, making photocatalytic reactions possible under visible light.

The reaction mechanism for H_2O with the $(\text{TiO}_2)_n$ ($n = 1\text{--}4$) nanoclusters has been studied using CCSD(T) and DFT.²⁴ This study showed that H_2O readily reacts with both the singlet and triplet states of TiO_2 nanoclusters to form the hydroxides. The reaction barriers are 5–16 kcal/mol for the singlet states and 5–26 kcal/mol for the triplet states for the first hydrolysis step. The first H_2O adsorption (physisorption) energies for the TiO_2 nanoclusters were calculated to be -10 to -35 kcal/mol for the singlet states and -10 to -50 kcal/mol for the triplet states. These physisorption energies depend on the cluster size and the site of adsorption. In general, H_2O prefers to physisorb on the Ti site with one $\text{Ti}=\text{O}$ bond and two $\text{Ti}-\text{O}$ bonds and at the Ti site with no $\text{Ti}=\text{O}$ bond and three $\text{Ti}-\text{O}$ bonds. The first hydrolysis (dissociative chemisorption) reaction energies of the TiO_2 nanoclusters were calculated to be -20 to -70 kcal/mol for the singlet states and -15 to -80 kcal/mol for the triplet states.

In the current study following our previous work,²⁴ DFT²⁵ calculations are used to study the initial steps for the reaction of H_2O with the $(\text{MO}_2)_n$ ($\text{M} = \text{Zr}, \text{Hf}; n = 1\text{--}4$) nanoclusters. For the monomer and dimer, reactions of up to two water molecules were studied; the reactions of one water molecule with the trimer and tetramer were studied. The potential energy surfaces for the reactions of water on both the ground state singlet and first excited triplet were calculated. Physisorption energies, hydrolysis reaction energies (dissociative chemisorption energies), and reaction barriers have been calculated using the B3LYP functional.^{26,27} The DFT potential energy surface for the singlet state of the monomer was benchmarked by comparison with those calculated at the coupled cluster [CCSD(T)]^{28–30} level with core–valence and scalar relativistic

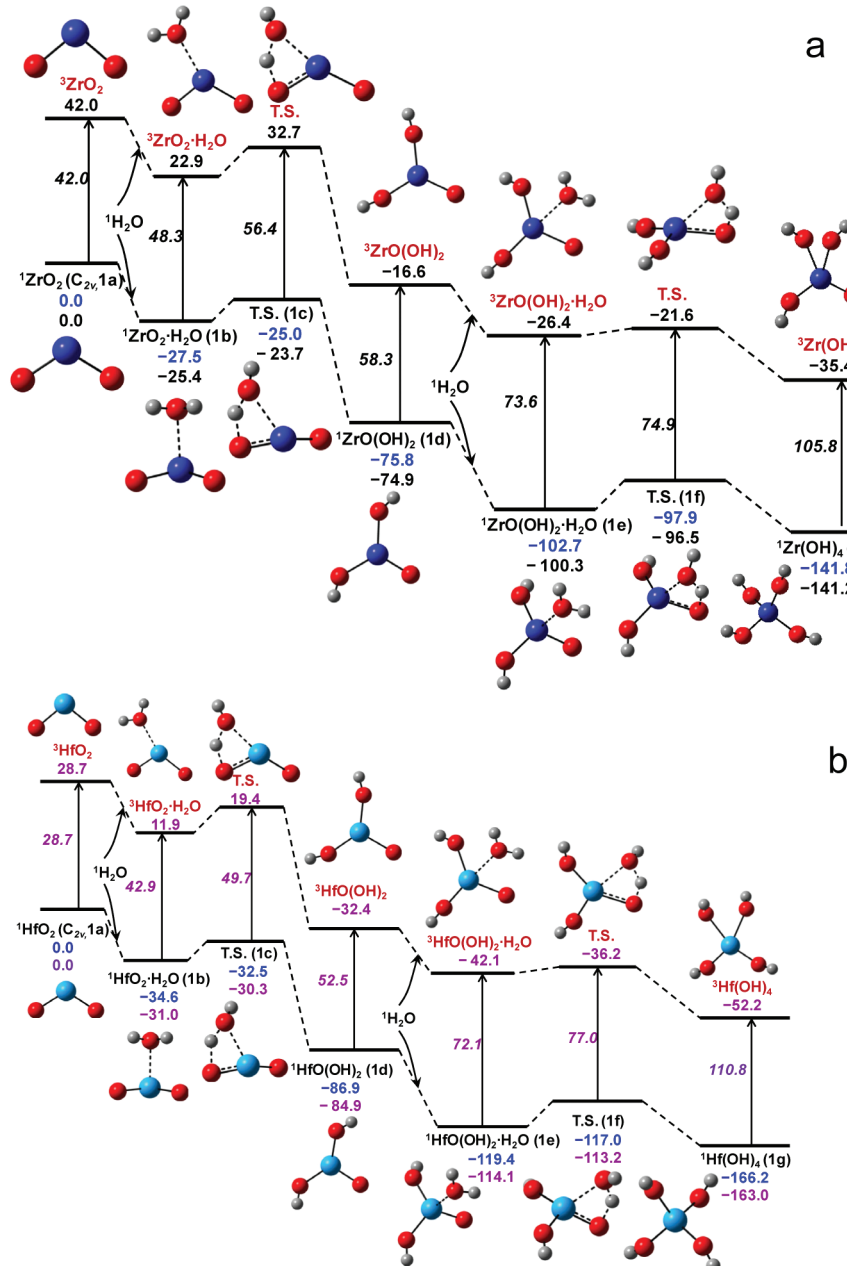


Figure 1. Potential energy surfaces for MO_2 (**1a**) + $2\text{H}_2\text{O} \rightarrow \text{MOH}_4$ at 0 K. Relative energies calculated at the CCSD(T)/CBS//B3LYP/aD (in blue) and B3LYP/aT//B3LYP/aD (in black for Zr and in purple for Hf) levels in kcal/mol. The O atoms are given in red, Zr atoms in dark blue, Hf atoms in blue, and H atoms in gray-white.

corrections using correlation-consistent basis sets^{31,32} and the appropriate pseudopotentials (PP).

COMPUTATIONAL METHODS

Geometries were optimized at the DFT level with the B3LYP exchange-correlation functional. Vibrational frequencies were calculated to characterize the stationary points located on the potential energy surface and to obtain the zero-point energy corrections (ZPEs) as well as the thermal and free energy corrections at 298 K, which were obtained by the normal statistical mechanical expressions.³³ For the triplet states with symmetry breaking at the B3LYP level, the BP86 exchange-correlation functional^{34,35} was used to calculate the ZPEs. These ZPEs were combined with the symmetry-constrained B3LYP energies to obtain the total energies. These functionals

were chosen based on our previous work on the ZrO_2 and HfO_2 nanoclusters²² and on the hydrolysis of TiO_2 nanoclusters.²⁴ The aug-cc-pVXZ basis sets³¹ for O and H and PP-based aug-cc-pVXZ-PP basis sets³² for Zr and Hf were used for the DFT geometry optimization and frequency calculations with X = D and for the DFT single-point energy calculations with X = T. For simplicity, we denote these combined basis sets as aX. The synchronous transit-guided quasi-Newton (STQN) method was used to find the transition states, which are characterized by a single imaginary frequency.³⁶ The DFT calculations were carried out with the Gaussian 09 program package.³⁷

For the singlet monomer potential energy surface, the B3LYP/aD geometries were used in single-point energy calculations at the coupled cluster [CCSD(T)] level^{28–30}

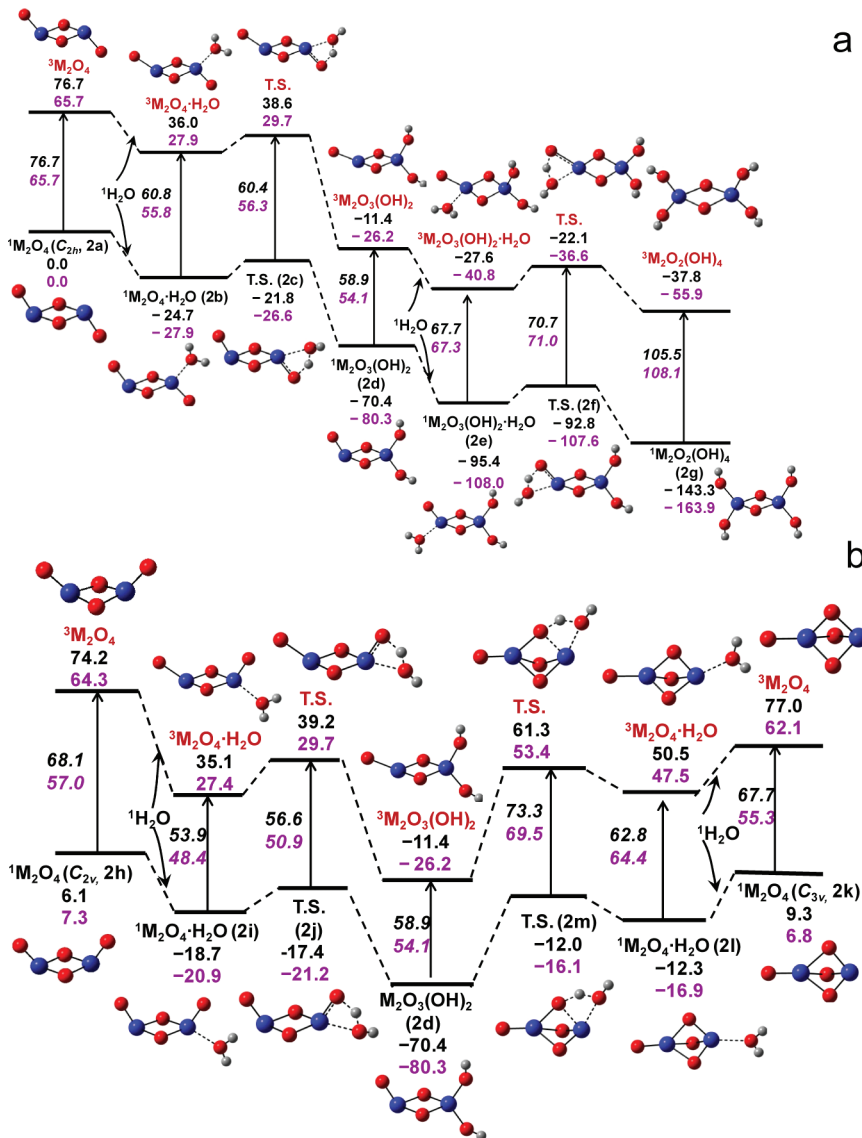


Figure 2. Potential energy surfaces for (a) $\text{M}_2\text{O}_4(\text{C}_{2h}, 2\text{a}) + 2\text{H}_2\text{O} \rightarrow \text{M}_2\text{O}_2(\text{OH})_4$ and (b) $\text{M}_2\text{O}_4(\text{C}_{2v}, 2\text{h}) + \text{H}_2\text{O} \rightarrow \text{M}_2\text{O}_3(\text{OH})_2$ and $\text{M}_2\text{O}_4(\text{C}_{3v}, 2\text{k}) + \text{H}_2\text{O} \rightarrow \text{M}_2\text{O}_3(\text{OH})_2$ at 0 K. Relative energies calculated at the B3LYP/aT//B3LYP/aD (in black for Zr and in purple for Hf) level in kcal/mol. See the Supporting Information for molecular structures for Hf.

with the sequence of basis sets of aX (X = D, T, and Q). These CCSD(T) energies were extrapolated to the complete basis set (CBS) limit using a mixed Gaussian/exponential formula.³⁸ Core-valence correlation corrections for the 1s² electrons on O and (n - 1)s²(n - 1)p⁶ electrons for Zr (n = 4) and Hf (n = 5) were calculated at the CCSD(T) level with the aug-cc-pwCVTZ basis set for O and the aug-cc-pwCVTZ-PP basis set for Zr and Hf;³⁹ these combined basis sets will be denoted as awCVTZ. Scalar relativistic corrections were calculated as the expectation values of the mass-velocity and Darwin operators (MVD) from the Breit-Pauli Hamiltonian for the CISD (configuration interaction with single and double excitations) wave function with the aT basis set. Following our previous work,⁴⁰ the pseudopotential corrections were calculated with the second-order Douglas-Kroll-Hess Hamiltonian⁴¹ and the all-electron aug-cc-pwCVTZ-DK basis set;^{42–44} these basis sets will be collectively denoted as awCVTZ-DK. For Hf, the 4f electrons are also correlated by including additional high angular momentum functions (2f, 2g, 1h), as the 4f electrons are higher in energy than the metal 5s and 5p electrons and

close to the O 2s electrons. All CCSD(T) calculations were performed with the MOLPRO 2010.1 program.⁴⁵

The calculations were performed on the local Xeon and Opteron based Penguin Computing clusters, the Xeon based Dell Linux cluster at the University of Alabama, the Opteron and Xeon based Dense Memory Cluster (DMC) and Itanium 2 based SGI Altix systems at the Alabama Supercomputer Center, and the Opteron based HP Linux cluster at the Molecular Science Computing Facility at Pacific Northwest National Laboratory. Molecular visualization was done using the AGUI graphics program from the AMPAC program package.⁴⁶

RESULTS

Cluster Geometries. The structures of the optimized hydroxides, hydrates, and transition states for the hydrolysis of $(\text{ZrO}_2)_n$ (n = 1–4) and HfO_2 are shown in Figures 1–9. The structures for the hydrolysis of dimers, trimers, and tetramers for M = Hf are shown in the Supporting Information. The total energies, Cartesian coordinates, calculated spin densities,

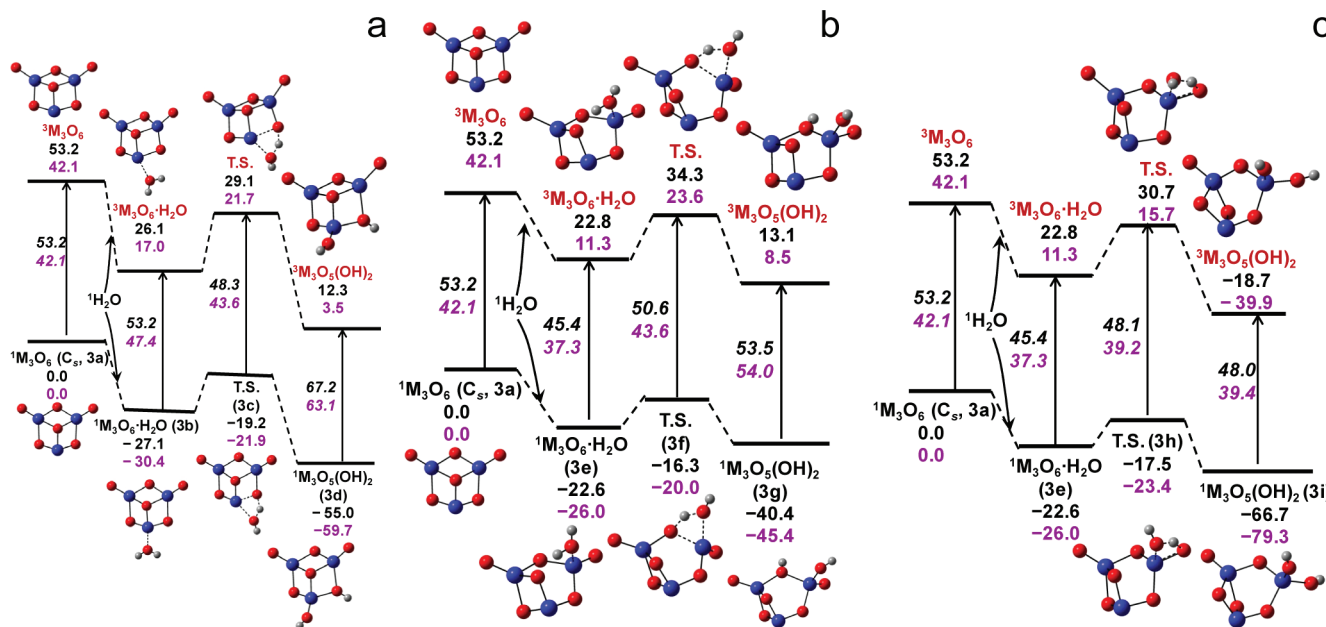


Figure 3. Potential energy surfaces for M_3O_6 (C_s , 3a) + $\text{H}_2\text{O} \rightarrow \text{M}_3\text{O}_5(\text{OH})_2$ at 0 K. Relative energies calculated at the B3LYP/aT//B3LYP/aD level in kcal/mol.

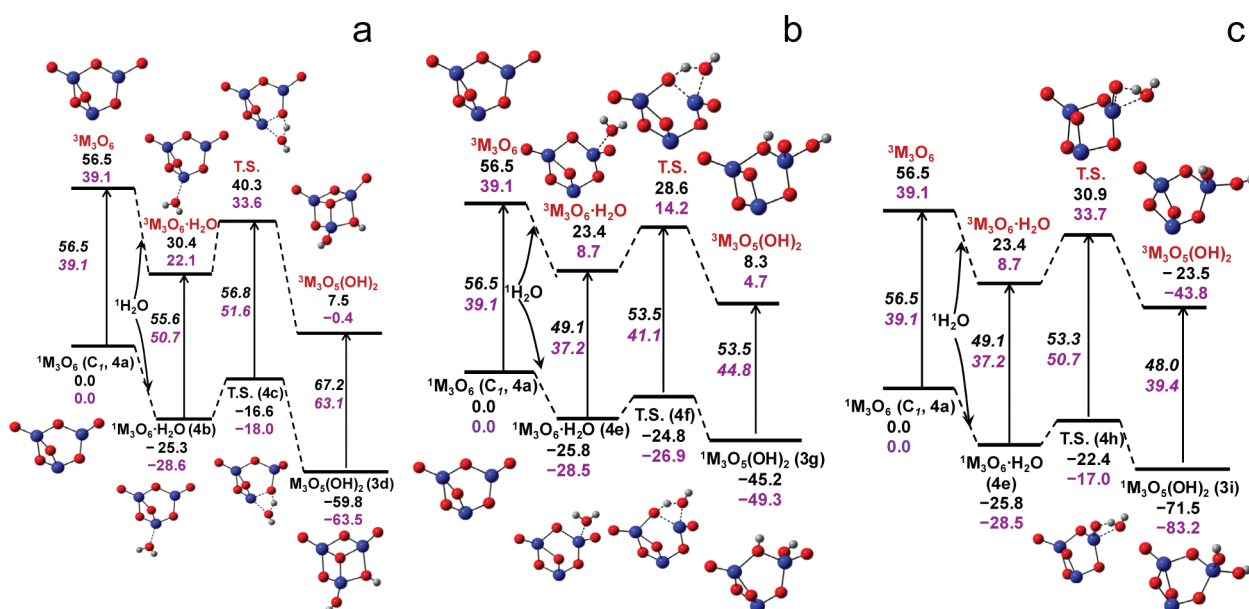


Figure 4. Potential energy surfaces for M_3O_6 (C_1 , 4a) + $\text{H}_2\text{O} \rightarrow \text{M}_3\text{O}_5(\text{OH})_2$ at 0 K. Relative energies calculated at the B3LYP/aT//B3LYP/aD level in kcal/mol.

harmonic frequencies, and the atomic numbering are also given in the Supporting Information.

Triplet States. In contrast to the C_s geometry of ${}^1\text{MO}(\text{OH})_2$, the ${}^3\text{MO}(\text{OH})_2$ (**1d**) structures are calculated to be planar with C_{2v} symmetry with M–OH bond distances of 1.948 and 1.924 Å, respectively, for M = Zr and Hf. As in our previous work on the hydrolysis of TiO_2 nanoclusters,²⁴ Jahn–Teller distortions are found for the triplet states of $\text{Zr}(\text{OH})_4$ and $\text{Hf}(\text{OH})_4$ (**1g**). There are two long Zr–OH bonds of 2.177 Å with $\angle \text{O–Zr–O} = 60.0^\circ$ and two short Zr–OH bonds of 1.951 Å with $\angle \text{O–Zr–O} = 117.6^\circ$. The respective bond distances for ${}^3\text{Hf}(\text{OH})_4$ are 2.143 and 1.931 Å, and the bond angles are 61.0° and 108.4° . The triplet states of $\text{Zr}_2\text{O}_2(\text{OH})_4$ and $\text{Hf}_2\text{O}_2(\text{OH})_4$ (**2g**) are calculated to have C_{2v} symmetry.

Singlet–Triplet Energy Gaps. The calculated excitation energies for the hydroxides are presented in Figures 1–9. The excitation energies for $\text{MO}(\text{OH})_2$ are higher than that for MO_2 by 16 kcal/mol for M = Zr and by 24 kcal/mol for M = Hf and are lower than that for $\text{M}(\text{OH})_4$ by 48 kcal/mol for M = Zr and by 58 kcal/mol for M = Hf. For $\text{M}_2\text{O}_2(\text{OH})_4$, the excitation energy is very close to that of $\text{M}(\text{OH})_4$. The excitation energy of HfO_2 is 14 kcal/mol lower than that of ZrO_2 , and the excitation energy difference between $\text{ZrO}(\text{OH})_2$ and $\text{HfO}(\text{OH})_2$ decreases to 6 kcal/mol. The differences in the excitation energies for $\text{Hf}(\text{OH})_4$ and $\text{Zr}(\text{OH})_4$ and $\text{Hf}_2\text{O}_2(\text{OH})_4$ and $\text{Zr}_2\text{O}_2(\text{OH})_4$ are even smaller, 5 and 3 kcal/mol, respectively.

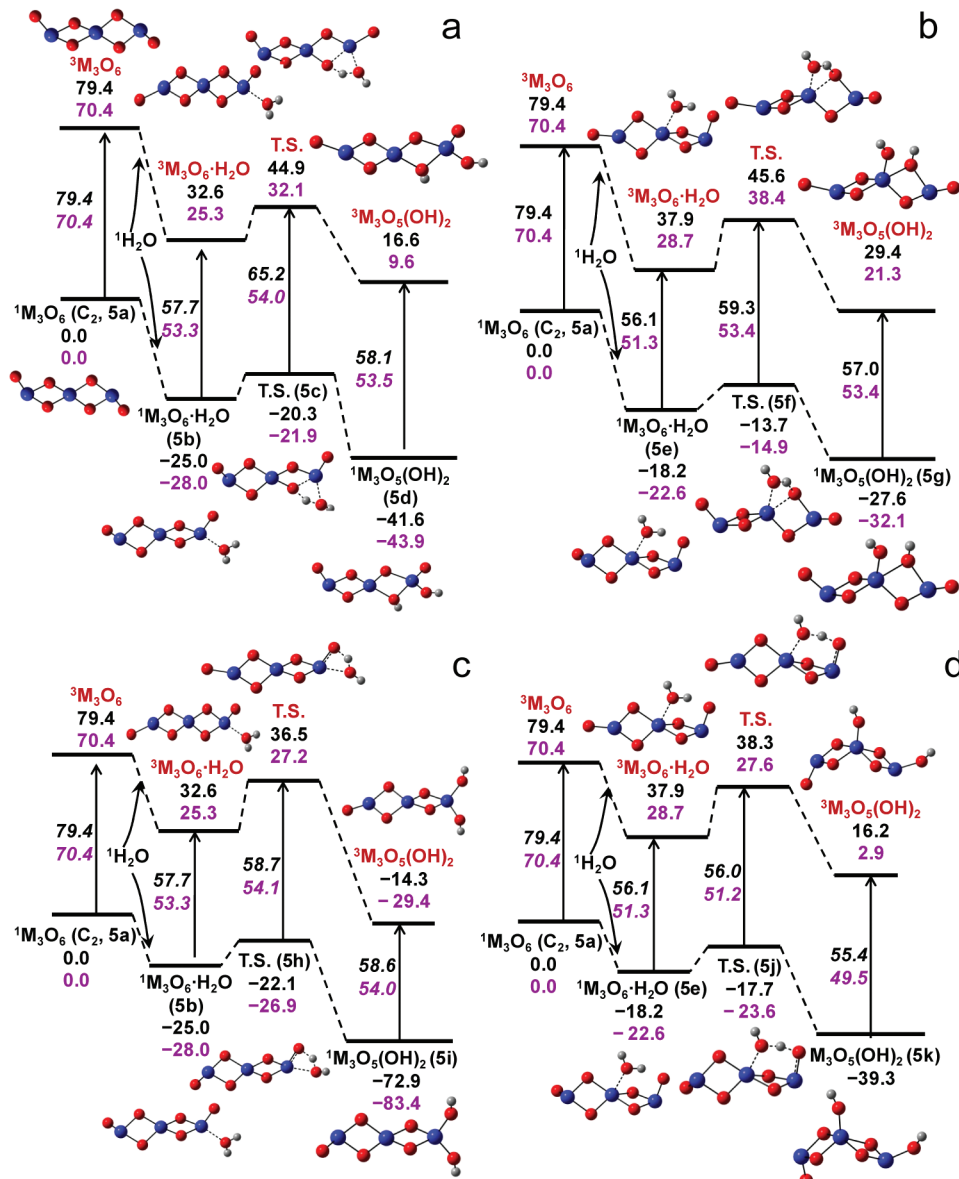


Figure 5. Potential energy surfaces for $\text{M}_3\text{O}_6(\text{C}_2, 5\text{a}) + \text{H}_2\text{O} \rightarrow \text{M}_3\text{O}_5(\text{OH})_2$ at 0 K. Relative energies calculated at the B3LYP/aT//B3LYP/aD level in kcal/mol.

The excitation energies of the different isomers of $\text{Zr}_3\text{O}_5(\text{OH})_2$, **3d**, **3g**, **3i**, **5d**, **5g**, **5i**, **5k**, **5d**, and **6f**, are calculated to be between 40 and 65 kcal/mol, depending on the structure of the isomer. The excitation energies for the different isomers of $\text{Hf}_3\text{O}_5(\text{OH})_2$ fall into the same range. For the hydrolysis of the tetramers, the excitation energies for $\text{Zr}_4\text{O}_7(\text{OH})_2$ (**7d**, **7g**, **7i**, **8d**, **8i**, **9i**) are calculated to be 50–77 kcal/mol, and those for $\text{Zr}_4\text{O}_7(\text{OH})_2$ (**9d**) and $\text{Zr}_4\text{O}_7(\text{OH})_2$ (**9g**) are calculated to be 36 and 27 kcal/mol, respectively. For $\text{M} = \text{Hf}$, the excitation energies are, in general, between 50 and 65 kcal/mol with two exceptions, $\text{Hf}_4\text{O}_7(\text{OH})_2$ (**9d**) and $\text{Hf}_4\text{O}_7(\text{OH})_2$ (**9g**), with excitation energies of only 29 and 18 kcal/mol, respectively. In general, the excitation energies for $\text{Zr}_4\text{O}_7(\text{OH})_2$ are 2–25 kcal/mol higher than those for the corresponding $\text{Hf}_4\text{O}_7(\text{OH})_2$ isomers depending on the different structures.

Hydrolysis Potential Energy Surfaces. The calculated potential energy surfaces for the hydrolysis of the $(\text{MO}_2)_n$ ($\text{M} = \text{Zr}, \text{Hf}$, $n = 1–4$) nanoclusters are shown in Figures 1–9.

Important energetic quantities are summarized in Tables 1 and 2.

Monomer. The potential energy surface for the hydrolysis of ${}^1\text{ZrO}_2$ calculated at the CCSD(T)/CBS level is shown in Figure 1. The hydrolysis reaction begins with an exothermic addition (physisorption) of H_2O to ZrO_2 to form a stable complex, $\text{ZrO}_2 \cdot \text{H}_2\text{O}$, with a Lewis acid–base donor–acceptor bond. A H atom migrates from the H_2O to a terminal $=\text{O}$ atom of the nanocluster, leading to the formation of two $\text{Zr}-\text{OH}$ bonds. The reaction energy barrier from $\text{ZrO}_2 \cdot \text{H}_2\text{O}$ is calculated to be very small. The reaction energy from $\text{ZrO}_2 \cdot \text{H}_2\text{O}$ to $\text{ZrO}(\text{OH})_2$ is quite exothermic, and the total dissociative chemisorption energy is –75.8 kcal/mol. The addition of a second H_2O molecule also forms a stable complex, $\text{ZrO}(\text{OH})_2 \cdot \text{H}_2\text{O}$, with a comparable physisorption energy. A H atom migrates from the H_2O again to form two additional $\text{Zr}-\text{OH}$ bonds. The reaction barrier for the second hydrogen transfer step from $\text{ZrO}(\text{OH})_2 \cdot \text{H}_2\text{O}$ is also small. The reaction energy from $\text{ZrO}(\text{OH})_2 \cdot \text{H}_2\text{O}$ to $\text{Zr}(\text{OH})_4$ is exothermic, giving a dissociative

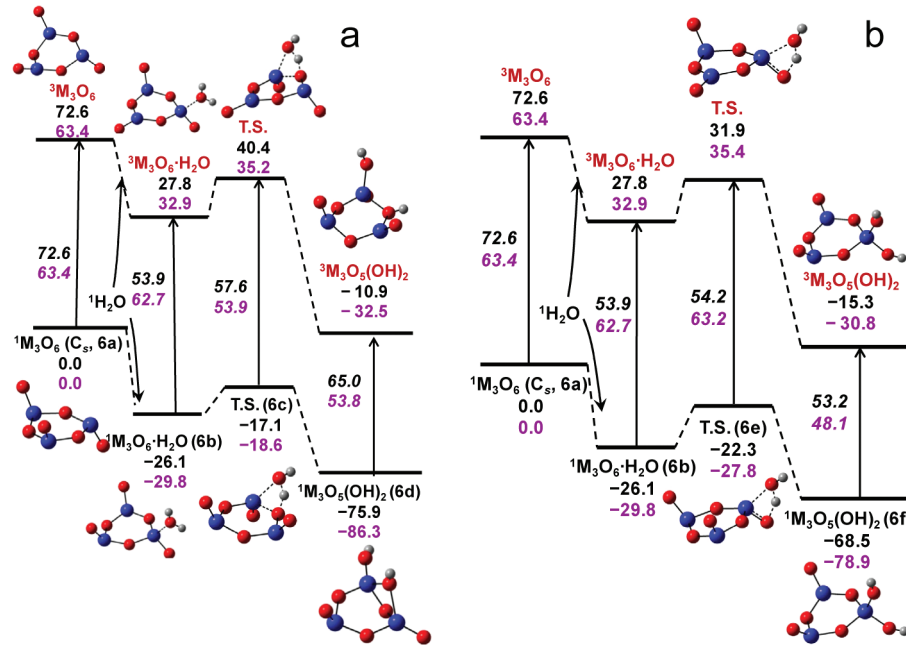


Figure 6. Potential energy surfaces for M_3O_6 (C_s , 6a) + $\text{H}_2\text{O} \rightarrow \text{M}_3\text{O}_5(\text{OH})_2$ at 0 K. Relative energies calculated at the B3LYP/aT//B3LYP/aD level in kcal/mol.

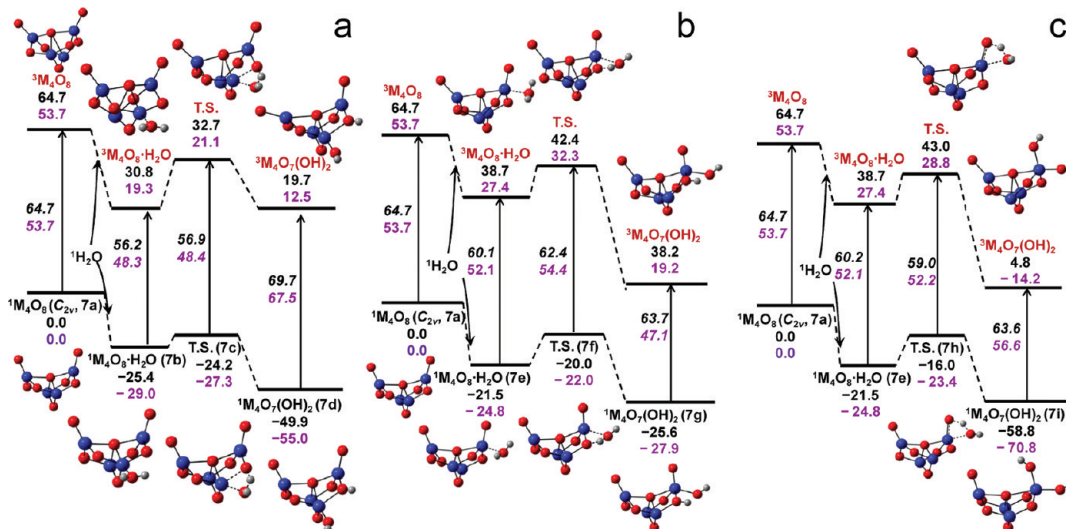


Figure 7. Potential energy surfaces for M_4O_8 (C_{2v} , 7a) + $\text{H}_2\text{O} \rightarrow \text{M}_4\text{O}_7(\text{OH})_2$ at 0 K. Relative energies calculated at the B3LYP/aT//B3LYP/aD level in kcal/mol.

chemisorption energy for the second water addition of -66.0 kcal/mol. The B3LYP/aT//B3LYP/aD potential energy surface (Figure 1) is in semiquantitative agreement with the CCSD(T)/CBS potential energy surface, within 3 kcal/mol.

The potential energy surface for the hydrolysis of ${}^3\text{ZrO}_2$ at the B3LYP/aT//B3LYP/aD level is also given in Figure 1 and is similar to the hydrolysis of the singlet state. The physisorption energy for the addition of the first H_2O to ${}^3\text{ZrO}_2$ is 6.3 kcal/mol less than that for the singlet. The reaction energy for ${}^3\text{ZrO}_2$ with two H_2O to form ${}^3\text{Zr}(\text{OH})_4$ is exothermic by only one-half of that for the singlet state. The first reaction barrier (${}^3\text{ZrO}_2 \cdot \text{H}_2\text{O} \rightarrow {}^3\text{ZrO}(\text{OH})_2$) is much higher in the triplet than in the singlet. The second reaction barrier (${}^3\text{ZrO}(\text{OH})_2 \cdot \text{H}_2\text{O} \rightarrow {}^3\text{Zr}(\text{OH})_4$) is comparable to that on the singlet surface.

The potential energy surfaces for the hydrolysis of both ${}^1\text{HfO}_2$ and ${}^3\text{HfO}_2$ at the CCSD(T)/CBS level and B3LYP/aT//B3LYP/aD levels are shown in Figure 1. The hydrolysis of HfO_2 is similar to that of ZrO_2 with the same overall qualitative reaction path. The physisorption and dissociative chemisorption energies are calculated to be more negative for HfO_2 than for ZrO_2 . For the hydrolysis of ${}^3\text{HfO}_2$, the reaction ${}^3\text{HfO}_2 \cdot \text{H}_2\text{O} \rightarrow {}^3\text{HfO}(\text{OH})_2$ is quite exothermic, and the reaction barrier is higher than in the singlet. The potential energy surface at the B3LYP/aT//B3LYP/aD level is in semiquantitative agreement with the CCSD(T)/CBS potential energy surface with energy differences less than 5 kcal/mol.

The results in Figure 1 show that H_2O should react *readily* with both the ground and first triplet excited states of MO_2 ($\text{M} = \text{Zr}, \text{Hf}$) with reaction barriers that are less than 10 kcal/mol.

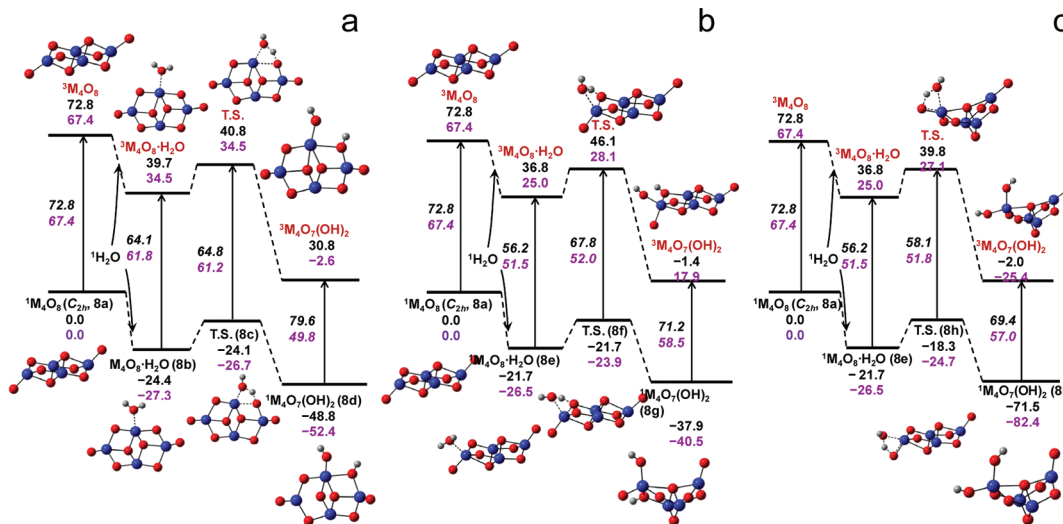


Figure 8. Potential energy surfaces for M_4O_8 (C_{2h} , 8a) + $\text{H}_2\text{O} \rightarrow \text{M}_4\text{O}_7(\text{OH})_2$ at 0 K. Relative energies calculated at the B3LYP/aT//B3LYP/aD level in kcal/mol.

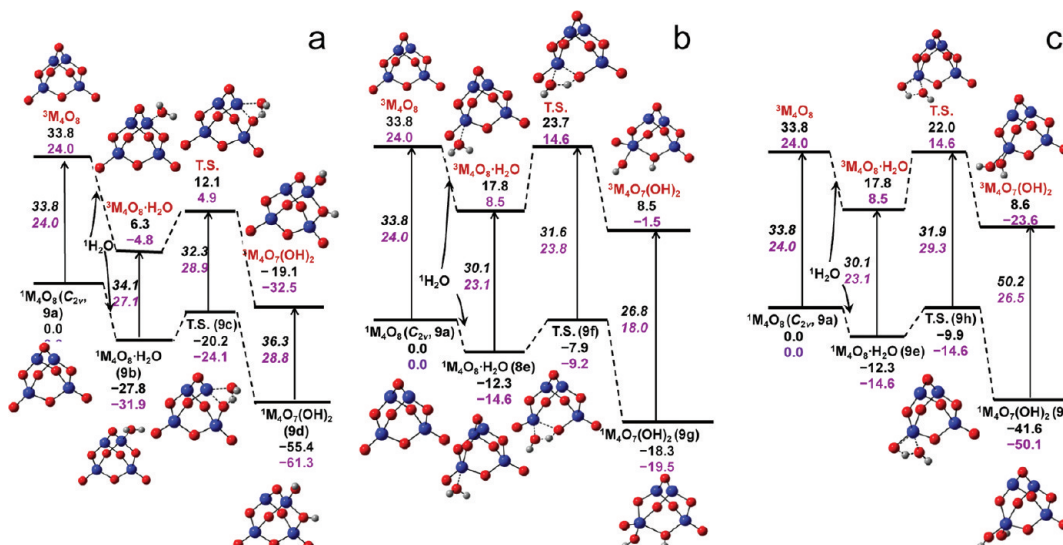


Figure 9. Potential energy surfaces for M_4O_8 (C_{2v} , 9a) + $\text{H}_2\text{O} \rightarrow \text{M}_4\text{O}_7(\text{OH})_2$ at 0 K. Relative energies calculated at the B3LYP/aT//B3LYP/aD level in kcal/mol.

Dimer. The potential energy surfaces for the hydrolysis of Zr_2O_4 and Hf_2O_4 for the addition of two water molecules are shown in Figure 2. After the first hydrolysis step for the three isomers, the same structure of the hydroxide, $\text{M}_2\text{O}_3(\text{OH})_2$ (2d), is formed. The hydrolysis reaction for the addition of two H_2O molecules is highly exothermic for both the singlet and triplet states. For Zr_2O_4 (2a) and (2h), after forming the stable $\text{Zr}_2\text{O}_4\cdot\text{H}_2\text{O}$ complex, a H atom transfers from H_2O to a terminal $=\text{O}$ atom to form two $\text{Zr}-\text{OH}$ bonds with very small barriers from the complex. The calculated reaction energy for the transformation of $\text{Zr}_2\text{O}_4\cdot\text{H}_2\text{O}$ into $\text{Zr}_2\text{O}_3(\text{OH})_2$ is substantially exothermic. For the hydrolysis of Zr_2O_4 (2k), the H transfers to a bridge $-\text{O}$, and the $\text{Zr}-\text{O}-\text{Zr}$ bonds are broken to form two $\text{Zr}-\text{OH}$ bonds with a reaction barrier of only 0.3 kcal/mol.

The hydrolysis reaction of Hf_2O_4 is similar to that of Zr_2O_4 . For the singlet state, the reaction barriers for the first step are calculated to be between 0 and 3 kcal/mol. The reaction energies from the complex for the first step are between -50

and -60 kcal/mol, and the reaction energy for the second step is -55.9 kcal/mol. For the triplet state, the reaction barriers for the first step are calculated to be between 2 and 6 kcal/mol. The reaction energies from the complex for the first step are between -50 and -70 kcal/mol, and the reaction energy for the second step is -15.9 kcal/mol.

Trimer. The potential energy surfaces for the hydrolysis of M_3O_6 with a single water molecule are given in Figures 3–6. For the four different isomers, M_3O_6 (3a, 4a, 5a, 6a), hydrolysis of the metal center with and without a terminal oxygen atom was examined. For the metal center with a terminal oxygen atom, the migration of a hydrogen atom to both a terminal $=\text{O}$ atom and to a bridge $-\text{O}$ atom was studied. After the addition of H_2O to M_3O_6 (C₁, 4a), the hydrolysis products $\text{M}_3\text{O}_5(\text{OH})_2$ are the same as that of M_3O_6 (C₁, 3a).

For ${}^1\text{Zr}_3\text{O}_6$, the reaction barriers are calculated to be 1–9 kcal/mol, and the overall reaction energies are quite exothermic by -40 to -75 kcal/mol depending on the different isomers, water attachment locations, and different H migrations. The

Table 1. Calculated Lewis Acidities (Fluoride Affinities or FA, kcal/mol, ΔH_{298K}), Reaction Barriers from the Reactant Complexes (ΔH_{298K}^\ddagger , kcal/mol), Imaginary Frequencies for the Transition States (ω_e , cm⁻¹), and Physisorption and Dissociative Chemisorption Enthalpies ($\Delta H_{ad,298K}$, kcal/mol) for the First Addition of H₂O at the B3LYP/aT//B3LYP/aD Level^a

reaction	FA	ΔH_{298K}^\ddagger		$\omega_e(i)$		$\Delta H_{ad,298K}$ (physisorption)		$\Delta H_{ad,298K}$ (chemisorption)	
		singlet	triplet	singlet	triplet	singlet	triplet	singlet	triplet
ZrO ₂ (1a) + H ₂ O → ZrO(OH) ₂ (1d)	105.8	0.9	8.7	1177.7	1493.1	-26.0	-19.2	-75.5	-59.0
Zr ₂ O ₄ (<i>C</i> _{2h} , 2a) + H ₂ O → Zr ₂ O ₃ (OH) ₂ (2d)	112.0	2.1	2.4	1222.1	1263.0	-25.0	-40.4	-70.6	-87.4
Zr ₂ O ₄ (<i>C</i> _{2v} , 2h) + H ₂ O → Zr ₂ O ₃ (OH) ₂ (2d)	115.4	0.6	3.5	1136.0	1266.3	-25.2	-38.5	-76.8	-85.7
Zr ₂ O ₄ (<i>C</i> _{3v} , 2k) + H ₂ O → Zr ₂ O ₃ (OH) ₂ (2d)	124.0 ^b	0.0	9.8	926.0	1306.6	-21.6	-25.3	-79.9	-86.6
Zr ₃ O ₆ (<i>C</i> _s , 3a) + H ₂ O → Zr ₃ O ₅ (OH) ₂ (3d)	143.0	7.1	2.2	1267.3	1034.5	-27.3	-27.7	-55.4	-41.4
Zr ₃ O ₆ (<i>C</i> _s , 3a) + H ₂ O → Zr ₃ O ₅ (OH) ₂ (3g)	109.0	6.0	11.1	1189.7	1165.0	-23.4	-31.2	-40.8	-40.7
Zr ₃ O ₆ (<i>C</i> _s , 3a) + H ₂ O → Zr ₃ O ₅ (OH) ₂ (3i)	109.0	4.7	7.3	1120.4	1234.5	-23.4	-31.2	-66.5	-71.9
Zr ₃ O ₆ (<i>C</i> _v , 4a) + H ₂ O → Zr ₃ O ₅ (OH) ₂ (3d)	148.0 ^c	7.9	9.2	1236.5	1247.5	-25.5	-26.4	-60.4	-49.7
Zr ₃ O ₆ (<i>C</i> _v , 4a) + H ₂ O → Zr ₃ O ₅ (OH) ₂ (3g)	114.0 ^d	0.3	4.5	965.3	1167.5	-26.6	-34.0	-45.8	-49.0
Zr ₃ O ₆ (<i>C</i> ₁ , 4a) + H ₂ O → Zr ₃ O ₅ (OH) ₂ (3i)	114.0	2.8	7.0	1272.2	1360.2	-26.6	-34.0	-71.5	-80.2
Zr ₃ O ₆ (<i>C</i> ₂ , 5a) + H ₂ O → Zr ₃ O ₅ (OH) ₂ (5d)	118.6	3.9	11.7	1109.4	994.7	-25.3	-47.2	-42.0	-63.3
Zr ₃ O ₆ (<i>C</i> ₂ , 5a) + H ₂ O → Zr ₃ O ₅ (OH) ₂ (5g)	90.7	4.5	7.7	955.5	993.4	-19.3	-42.7	-28.0	-50.4
Zr ₃ O ₆ (<i>C</i> ₂ , 5a) + H ₂ O → Zr ₃ O ₅ (OH) ₂ (5i)	118.6	2.2	3.2	1221.8	1272.7	-25.3	-47.2	-73.0	-93.8
Zr ₃ O ₆ (<i>C</i> ₂ , 5a) + H ₂ O → Zr ₃ O ₅ (OH) ₂ (5k)	90.7	0.1	0.3	952.4	962.9	-19.3	-42.7	-39.3	-63.1
Zr ₃ O ₆ (<i>C</i> _s , 6a) + H ₂ O → Zr ₃ O ₅ (OH) ₂ (6d)	167.1 ^e	8.1	11.9	1194.1	1170.9	-26.4	-45.1	-76.7	-84.4
Zr ₃ O ₆ (<i>C</i> _s , 6a) + H ₂ O → Zr ₃ O ₅ (OH) ₂ (6f)	167.1 ^e	2.8	3.3	1263.1	1287.8	-26.4	-45.1	-68.7	-88.0
Zr ₄ O ₈ (<i>C</i> _{2v} , 7a) + H ₂ O → Zr ₄ O ₇ (OH) ₂ (7d)	131.4	0.4	1.1	937.3	906.5	-25.6	-34.7	-50.2	-45.8
Zr ₄ O ₈ (<i>C</i> _{2v} , 7a) + H ₂ O → Zr ₄ O ₇ (OH) ₂ (7g)	104.1	1.0	3.0	975.1	990.3	-22.1	-26.9	-26.0	-27.6
Zr ₄ O ₈ (<i>C</i> _{2v} , 7a) + H ₂ O → Zr ₄ O ₇ (OH) ₂ (7i)	104.1	4.9	3.6	1337.7	1320.1	-22.1	-26.9	-59.0	-60.5
Zr ₄ O ₈ (<i>C</i> _{2h} , 8a) + H ₂ O → Zr ₄ O ₇ (OH) ₂ (8d)	124.8	0.0	0.3	728.1	958.4	-24.9	-33.8	-49.4	-42.5
Zr ₄ O ₈ (<i>C</i> _{2h} , 8a) + H ₂ O → Zr ₄ O ₇ (OH) ₂ (8g)	118.5	0.0	10.9	955.9	986.6	-22.5	-39.0	-38.5	-40.3
Zr ₄ O ₈ (<i>C</i> _{2h} , 8a) + H ₂ O → Zr ₄ O ₇ (OH) ₂ (8i)	118.5	3.0	3.4	1295.9	1171.5	-22.5	-39.0	-71.9	-75.4
Zr ₄ O ₈ (<i>C</i> _{2v} , 9a) + H ₂ O → Zr ₄ O ₇ (OH) ₂ (9d)	139.1	6.7	4.5	1337.5	1268.2	-28.0	-28.0	-55.8	-53.5
Zr ₄ O ₈ (<i>C</i> _{2v} , 9a) + H ₂ O → Zr ₄ O ₇ (OH) ₂ (9g)	70.0	3.9	5.4	1040.6	1208.9	-12.9	-16.9	-18.8	-26.0
Zr ₄ O ₈ (<i>C</i> _{2v} , 9a) + H ₂ O → Zr ₄ O ₇ (OH) ₂ (9i)	70.0	1.8	3.6	1249.4	1319.1	-12.9	-16.9	-41.8	-25.5

^aSee Figures 1–9 and Supporting Information for the molecular structures of the reactants, transition states, and products. For the reactions involving the triplet states, H₂O is in the singlet state. For the fluoride affinity, the reaction site is the same as that involved in the hydrolysis reaction.

^bUpon the addition of the F⁻ anion, the cluster structure is changed into that for Zr₂O₄ (*C*_{2h}, **2a**) + H₂O → Zr₂O₃(OH)₂ (**2d**). ^cUpon the addition of the F⁻ anion, the cluster structure is changed into that for Zr₃O₆ (*C*_s, **3a**) + H₂O → Zr₃O₅(OH)₂ (**3d**). ^dUpon the addition of the F⁻ anion, the cluster structure is changed into that for Zr₃O₆ (*C*_s, **3a**) + H₂O → Zr₃O₅(OH)₂ (**3g**). ^eUpon the addition of the F⁻ anion, the cluster structure is changed into that for Zr₃O₆ (*C*_s, **3a**) + H₂O → Zr₃O₅(OH)₂ (**3d**).

barriers and overall reaction energies for the hydrolysis of ³Zr₃O₆ fall into the range of 1–13 kcal/mol and -40 to -94 kcal/mol. For the hydrolysis of singlet Hf₃O₆, the reaction barriers are calculated to be between 0 and 11 kcal/mol, and overall reaction energies are calculated to be -32 to -86 kcal/mol. For ³Hf₃O₆, the reaction barriers are calculated to be between 0 and 11 kcal/mol, and the overall reaction energies are calculated to be -35 to -100 kcal/mol. All of the reactions of the trimers have very low reaction barriers. These reaction barriers are nearly 0 for both singlet and triplet states for the reaction of M₃O₆ (*C*₂, **5a**) + H₂O → M₃O₅(OH)₂ (**5k**). When water is attached to the metal bonded to a terminal oxygen, the overall reaction energies for H migration to a terminal =O are more exothermic than for H migration to a bridge -O.

Tetramer. The potential energy surfaces for the first hydrolysis steps of M₄O₈ are given in Figures 7–9. Like the hydrolysis of the trimers, H transfer steps to both a terminal =O atom and a bridge -O atom were studied. For the singlet states of Zr₄O₈, the reaction barriers are calculated to be 0–8 kcal/mol, and the overall reaction energies are exothermic by -19 to -50 kcal/mol. The barriers and overall reaction energies for the hydrolysis of ³Zr₄O₈ fall in the ranges of 1–11 kcal/mol and -25 to -60 kcal/mol, respectively. For the hydrolysis of the singlet states of Hf₄O₈, the reaction barriers

are calculated to be between 0 and 8 kcal/mol, and the overall reaction energies are calculated to be -19 to -70 kcal/mol. For the hydrolysis of ³Hf₄O₈, the reaction barriers are calculated to be between 2 and 10 kcal/mol, and the overall reaction energies are calculated to be -25 to -70 kcal/mol. The reaction barriers for hydrolysis of the tetramers are quite small and fall into the same range as those for the trimers.

H₂O Physisorption Energies on MO₂ Nanoclusters.

The calculated physisorption energies for H₂O on (MO₂)_n (*n* = 1–4) nanoclusters at 298 K are given in Table 1 for M = Zr and Table 2 for M = Hf. The Mulliken populations on the metal are given in Table 4.

Singlet States. The adsorption energies for H₂O on ZrO₂ and HfO₂ at 0 K are calculated to be -27.5 and -34.6 kcal/mol at the CCSD(T)/CBS level. At the B3LYP/aT//B3LYP/aD level, the physisorption energies are -25.4 and -31.0 kcal/mol, respectively. These values are close to the adsorption energy for H₂O on TiO₂ at 0 K of -30.0 kcal/mol at the CCSD(T)-DK/awCVTZ-DK level. These interactions are typical of a Lewis acid–base interaction. The bond distances of ZrO₂–H₂O and HfO₂–H₂O bond distance results in a more negative physisorption energy. The Mulliken charge on Zr and Hf, 1.27e and 1.09e, shows that the interaction energy is not completely dominated

Table 2. Calculated Lewis Acidities (Fluoride Affinities or FA, kcal/mol, ΔH_{298K}), Reaction Barriers from the Reactant Complexes (ΔH_{298K}^\ddagger , kcal/mol), Imaginary Frequencies for the Transition States (ω_e , cm⁻¹), and Physisorption and Dissociative Chemisorption Enthalpies ($\Delta H_{ad,298K}$, kcal/mol) for the First Addition of H₂O at the B3LYP/aT//B3LYP/aD Level^a

reaction	FA	ΔH_{298K}^\ddagger		ω_e		$\Delta H_{ad,298K}$ (physisorption)		$\Delta H_{ad,298K}$ (chemisorption)	
		singlet	triplet	singlet	triplet	singlet	triplet	singlet	triplet
HfO ₂ (1a) + H ₂ O → HfO(OH) ₂ (1d)	113.4	0.0	6.7	1000.1	1445.2	-31.7	-17.5	-85.6	-61.7
Hf ₂ O ₄ (<i>C</i> _{2h} , 2a) + H ₂ O → Hf ₂ O ₃ (OH) ₂ (2d)	118.9	0.6	1.0	1003.7	1048.8	-28.3	-38.2	-80.6	-92.1
Hf ₂ O ₄ (<i>C</i> _{2v} , 2h) + H ₂ O → Hf ₂ O ₃ (OH) ₂ (2d)	122.5	0.0	1.3	822.1	1059.6	-28.5	-37.2	-87.9	-90.5
Hf ₂ O ₄ (<i>C</i> _{3v} , 2k) + H ₂ O → Hf ₂ O ₃ (OH) ₂ (2d)	131.5 ^b	0.0	5.1	921.2	1199.6	-23.7	-14.6	-87.4	-88.2
Hf ₃ O ₆ (<i>C</i> _g , 3a) + H ₂ O → Hf ₃ O ₅ (OH) ₂ (3d)	152.8	7.7	4.1	1263.9	1138.5	-30.7	-25.8	-60.1	-39.0
Hf ₃ O ₆ (<i>C</i> _g , 3a) + H ₂ O → Hf ₃ O ₅ (OH) ₂ (3g)	117.9	5.7	11.4	1200.4	1178.9	-26.8	-31.7	-45.9	-34.1
Hf ₃ O ₆ (<i>C</i> _g , 3a) + H ₂ O → Hf ₃ O ₅ (OH) ₂ (3i)	117.9	2.2	4.0	824.2	990.6	-26.8	-31.7	-79.2	-82.3
Hf ₃ O ₆ (<i>C</i> ₁ , 4a) + H ₂ O → Hf ₃ O ₅ (OH) ₂ (3d)	156.8 ^c	9.2	10.8	1252.2	1265.8	-28.8	-17.1	-64.1	-39.9
Hf ₃ O ₆ (<i>C</i> ₁ , 4a) + H ₂ O → Hf ₃ O ₅ (OH) ₂ (3g)	121.9 ^d	1.0	4.4	967.8	1154.9	-29.2	-26.8	-50.0	-35.0
Hf ₃ O ₆ (<i>C</i> ₁ , 4a) + H ₂ O → Hf ₃ O ₅ (OH) ₂ (3i)	121.9	0.2	7.5	1050.1	1385.0	-29.2	-26.8	-83.2	-83.2
Hf ₃ O ₆ (<i>C</i> ₂ , 5a) + H ₂ O → Hf ₃ O ₅ (OH) ₂ (5d)	124.5	5.3	5.9	1121.7	1152.0	-28.3	-45.4	-44.3	-61.2
Hf ₃ O ₆ (<i>C</i> ₂ , 5a) + H ₂ O → Hf ₃ O ₅ (OH) ₂ (5g)	97.2	7.6	9.7	915.1	1003.6	-23.8	-42.8	-32.4	-49.5
Hf ₃ O ₆ (<i>C</i> ₂ , 5a) + H ₂ O → Hf ₃ O ₅ (OH) ₂ (5i)	124.5	0.4	1.1	982.3	1061.1	-28.3	-45.4	-83.5	-99.8
Hf ₃ O ₆ (<i>C</i> ₂ , 5a) + H ₂ O → Hf ₃ O ₅ (OH) ₂ (5k)	97.2	0.0	0.0	722.6	762.8	-23.8	-42.8	-46.6	-67.4
Hf ₃ O ₆ (<i>C</i> _g , 6a) + H ₂ O → Hf ₃ O ₅ (OH) ₂ (6d)	179.1 ^e	10.4	1.6	1046.1	1185.8	-30.2	-30.9	-87.7	-96.6
Hf ₃ O ₆ (<i>C</i> _g , 6a) + H ₂ O → Hf ₃ O ₅ (OH) ₂ (6f)	179.1 ^e	1.1	1.7	1212.5	1113.7	-30.2	-30.9	-79.1	-94.2
Hf ₄ O ₈ (<i>C</i> _{2v} , 7a) + H ₂ O → Hf ₄ O ₇ (OH) ₂ (7d)	142.6	0.9	1.1	920.9	947.3	-29.3	-35.2	-55.3	-42.1
Hf ₄ O ₈ (<i>C</i> _{2v} , 7a) + H ₂ O → Hf ₄ O ₇ (OH) ₂ (7g)	112.9	2.1	4.3	977.3	1001.6	-25.3	-27.3	-28.3	-35.4
Hf ₄ O ₈ (<i>C</i> _{2v} , 7a) + H ₂ O → Hf ₄ O ₇ (OH) ₂ (7i)	112.9	0.8	0.9	1151.0	1129.0	-25.3	-27.3	-71.1	-68.6
Hf ₄ O ₈ (<i>C</i> _{2h} , 8a) + H ₂ O → Hf ₄ O ₇ (OH) ₂ (8d)	132.3	0.1	0.0	704.2	1042.2	-27.8	-33.7	-52.9	-70.8
Hf ₄ O ₈ (<i>C</i> _{2h} , 8a) + H ₂ O → Hf ₄ O ₇ (OH) ₂ (8g)	126.1	1.8	2.4	981.3	1039.8	-26.9	-43.4	-41.1	-50.5
Hf ₄ O ₈ (<i>C</i> _{2h} , 8a) + H ₂ O → Hf ₄ O ₇ (OH) ₂ (8i)	126.1	1.1	1.4	1073.8	703.8	-26.9	-43.4	-82.8	-93.5
Hf ₄ O ₈ (<i>C</i> _{2v} , 9a) + H ₂ O → Hf ₄ O ₇ (OH) ₂ (9d)	149.3	7.0	9.0	1324.9	1285.2	-32.1	-29.3	-61.7	-57.0
Hf ₄ O ₈ (<i>C</i> _{2v} , 9a) + H ₂ O → Hf ₄ O ₇ (OH) ₂ (9g)	72.5	4.9	5.6	1043.2	1199.5	-15.3	-16.2	-20.1	-26.1
Hf ₄ O ₈ (<i>C</i> _{2v} , 9a) + H ₂ O → Hf ₄ O ₇ (OH) ₂ (9i)	72.5	0.0	5.6	1063.5	1481.0	-15.3	-16.2	-50.4	-48.2

^aSee Figures 1–9 and Supporting Information for the molecular structures of the reactants, transition states, and products. For the reactions involving the triplet states, H₂O is in the singlet state. For the fluoride affinity, the reaction site is the same as that involved in the hydrolysis reaction.

^bUpon the addition of the F⁻ anion, the cluster structure is changed into that for Hf₂O₄ (*C*_{2h}, **2a**) + H₂O → Hf₂O₃(OH)₂ (**2d**). ^cUpon the addition of the F⁻ anion, the cluster structure is changed into that for Hf₃O₆ (*C*_g, **3a**) + H₂O → Hf₃O₅(OH)₂ (**3d**). ^dUpon the addition of the F⁻ anion, the cluster structure is changed into that for Hf₃O₆ (*C*_g, **3a**) + H₂O → Hf₃O₅(OH)₂ (**3g**). ^eUpon the addition of the F⁻ anion, the cluster structure is changed into that for Hf₃O₆ (*C*_g, **3a**) + H₂O → Hf₃O₅(OH)₂ (**3d**).

by the atomic charge on the metal site on MO₂ as M = Hf has the larger energy but smaller positive Mulliken charge.

The H₂O physisorption energies on the different M₂O₄ structures at 298 K are calculated to be -22 to -29 kcal/mol. For isomers **2a** and **2h**, the M₂O₄–H₂O bond distances differ by only ~0.003 Å, consistent with a slight difference in H₂O physisorption energies of only ~0.2 kcal/mol. The physisorption energies are 3–4 kcal/mol less negative for **2k** than those for **2a** and **2h**, consistent with its longer H₂O–M distance by ~0.15 Å. The Mulliken charges on Zr are calculated to be 1.41e, 1.41e, and 1.05e for **2a**, **2h**, and **2k**. These for M = Hf are 1.50e, 1.56e, and 1.63e, respectively. The **2h** isomer of Hf₂O₄ has a lower positive charge on Hf than does the **2k** isomer, but the **2h** isomer has a more negative H₂O physisorption energy, which again shows the interaction energy is not completely determined by the atomic charge on the metal site.

For the different trimer isomers, the physisorption energies are calculated to be -20 to -30 kcal/mol dependent on the different structures and adsorption sites. In general, the H₂O physisorption energies on the metal sites without an M=O bond are more negative than those on the metal sites with an M=O bond, for example, in the case of isomers **3a** and **5a**. However, the M₃O₆ **4a** isomer is an exception because the

M₃O₆–H₂O bond distance in isomer **4e** (2.34 Å for M = Zr, 2.29 Å for M = Hf) is shorter than that in **4b** (2.36 Å for M = Zr, 2.31 Å for M = Hf), and isomer **4e** has a higher atomic charge of the metal (1.56e for M = Zr, 2.08e for M = Hf) than does isomer **4b** (1.47e for M = Zr, 1.64e for M = Hf). For isomer **6a**, the Zr₃O₆–H₂O and Hf₃O₆–H₂O bond distances, 2.31 and 2.28 Å, lead to reasonable physisorption energies of -26.4 and -30.2 kcal/mol. For this case, H₂O adsorbs on the M=O(–O)₂ site.

The physisorption energies for the three different tetramers, **7a**, **8a**, and **9a**, fall in the range of -12 to -30 kcal/mol. These energies again depend on the different structures and adsorption sites. Similar to the physisorption energies for the trimers, those for the metal sites without an M=O bond are more negative than those on the metal sites with an M=O bond for all three isomers. The physisorption energy of H₂O on the metal site with an M=O bond in **9a** is found to be the least negative (-12.9 kcal/mol for M = Zr and -15.3 kcal/mol for M = Hf). The H₂O–M distances are up to 2.43 Å for M = Zr and 2.38 Å for M = Hf.

The physisorption energies are calculated to be generally between -25 and -30 kcal/mol for the M(IV) site with one M=O bond and two M–O bonds for M = Zr and Hf. The physisorption energy for the M(III) in M₂O₄ (**2k**) is less

Table 3. Calculated Metal (M = Zr, Hf) Terminal Oxygen Stretching Frequencies (cm^{-1}) at the B3LYP/aD Level

molecule ^a	M = Zr		M = Hf	
	ω_e (S) ^b	ω_e (T) ^c	ω_e (S) ^b	ω_e (T) ^c
MO_2 (1a) ^d	859.7, 924.3	481.1, 809.3	822.4, 907.7	517.2, 796.3
MO(OH)_2 (1d)	925.4	601.8	901.6	568.9
M_2O_4 (C_{2h} , 2a) ^d	902.6, 913.7	608.9, 689.0	883.2, 890.5	641.2, 737.3
M_2O_4 (C_{2v} , 2h)	901.3, 921.9	623.4, 709.8	883.9, 897.9	640.5 ^d , 719.5 ^d
M_2O_4 (C_{3v} , 2k)	899.8	587.5	879.2	581.2
M_2O_3 (OH_2) (2d)	912.1	565.7	888.7	556.7
M_3O_6 (C_s , 3a) ^d	896.2, 915.3	677.3, 685.8	876.3, 890.2	675.1, 699.3
M_3O_6 (C_1 , 4a)	899.2, 921.2	576.2, 906.7	876.8, 901.4	573.0, 907.6
M_3O_6 (C_2 , 5a)	912.9, 915.5	743.3	890.0, 891.7	747.9
M_3O_6 (C_s , 6a)	914.6, 914.9, 923.3	699.6, 921.3	896.7, 904.2, 906.4	721.8, 906.1
$\text{M}_3\text{O}_5(\text{OH})_2$ (3d)	903.2, 922.4	562.7, 912.9	882.4, 897.1	566.1, 887.4
$\text{M}_3\text{O}_5(\text{OH})_2$ (3g)	913.5, 920.0	589.4, 918.4	891.9, 897.4	576.1, 895.4
$\text{M}_3\text{O}_5(\text{OH})_2$ (3i)	902.3	578.2	876.8	571.8
$\text{M}_3\text{O}_5(\text{OH})_2$ (5d)	913.2, 925.1	573.7, 917.9	888.2, 902.4	563.5, 893.3
$\text{M}_3\text{O}_5(\text{OH})_2$ (5g)	906.0, 924.8	562.9, 927.8	882.1, 902.9	552.8, 907.4
$\text{M}_3\text{O}_5(\text{OH})_2$ (5i)	915.4	567.4	891.5	557.1
$\text{M}_3\text{O}_5(\text{OH})_2$ (5k)	894.2	554.6	865.8	550.2
$\text{M}_3\text{O}_5(\text{OH})_2$ (6d)	909.1, 921.7	593.9, 904.2, 923.4	868.0, 885.7	573.3, 890.0
$\text{M}_3\text{O}_5(\text{OH})_2$ (6f)	917.1, 926.4	485.5, 924.2	905.8, 906.2	577.1, 906.3
M_4O_8 (C_{2v} , 7a) ^d	914.0, 924.2	716.2, 739.3	893.5, 900.5	697.5, 750.8
M_4O_8 (C_{2v} , 8a) ^d	911.7, 915.9	691.2, 716.4	888.2, 891.4	701.4, 718.2
M_4O_8 (C_{2v} , 9a) ^d	893.9, 906.1	692.1, 761.0	875.6, 884.6	692.2, 768.0
$\text{M}_4\text{O}_7(\text{OH})_2$ (7d)	910.4, 926.7	581.7, 919.2	887.6, 904.5	577.8, 883.4
$\text{M}_4\text{O}_7(\text{OH})_2$ (7g)	918.0, 926.5	584.6, 914.0	895.1, 901.9	592.5, 890.2
$\text{M}_4\text{O}_7(\text{OH})_2$ (7i)	908.1	590.1	883.4	571.4
$\text{M}_4\text{O}_7(\text{OH})_2$ (8d)	913.1, 918.5	586.7, 905.4	889.0, 895.0	574.7, 892.3
$\text{M}_4\text{O}_7(\text{OH})_2$ (8g)	905.9, 920.1	610.7, 907.3	882.6, 895.3	570.6, 891.3
$\text{M}_4\text{O}_7(\text{OH})_2$ (8i)	908.1	585.2	883.4	568.7
$\text{M}_4\text{O}_7(\text{OH})_2$ (9d)	898.8, 910.4	574.0, 907.4	881.3, 887.1	563.2, 885.7
$\text{M}_4\text{O}_7(\text{OH})_2$ (9g)	906.5, 920.0	569.5, 909.8	890.1, 899.3	562.8, 888.8
$\text{M}_4\text{O}_7(\text{OH})_2$ (9i)	900.7	901.2	881.6	568.0

^aSee Figures 1–9 and Supporting Information for the molecular structures. ^bFor the singlet states. ^cFor the triplet states. ^dAt the BP86/aD level for the triplet state.

negative. The similar structures of **3a** and **4a** show different H_2O physisorption energies. For reaction $3\text{a} \rightarrow 3\text{d}$ where water binds to an M(III) site, two bicoordinate O atoms and one tricoordinate O atom together with the adsorbed O atom form a stable tetrahedral conformation, resulting in a more negative physisorption energy as compared to the similar reaction $4\text{a} \rightarrow 3\text{d}$. For $3\text{a} \rightarrow 3\text{e}$ where water binds to an M(IV) site, the restructuring of the central tricoordinate O atom to a bicoordinate O atom results in a less negative physisorption energy as compared to the similar process $4\text{a} \rightarrow 4\text{e}$ in which there is no restructuring. The process **5a** → **5e** is calculated to have the least negative energy compared to the other trimer reactions because the four bridging O atoms are constrained to be in a tetrahedral coordination and cannot distort to provide additional space for the adsorbed H_2O molecule. A similar steric constraint is found in the process **9a** → **9e**, which is calculated to have the least negative physisorption energy. In contrast, the M(III) site in M_4O_8 (**9a**) with three M–O bonds is sterically flexible and has the most negative physisorption energy. The physisorption energies on the M(IV) sites in **7a** and **8a**, either bonded with four bridge O atoms or bonded with one terminal O atom and three bridge O atoms, are calculated to be –20 and –30 kcal/mol.

Triplet States. The triplet state of MO_2 has a less negative physisorption energy than the singlet state by 6.8 kcal/mol for

M = Zr and 14.2 kcal/mol for M = Hf. These energy differences are mainly due to the lower partial charge on the metal, 0.98e for M = Zr and 0.90e for M = Hf as compared to the respective singlet values of 1.27 and 1.09e. The Zr– H_2O and Hf– H_2O bond distances are 2.34 and 2.31 Å, somewhat longer than those of the singlet states. The less negative energies associated with the triplets for ZrO_2 and HfO_2 are consistent with our previous studies on TiO_2 .²⁴

The H_2O physisorption energies for the triplet of the dimers are from –15 to –40 kcal/mol. The triplet states of the isomers **2a** and **2h** have more negative adsorption energies than the singlet states by ~15 kcal/mol for M = Zr and ~10 kcal/mol for M = Hf. ${}^3\text{Zr}_2\text{O}_4$ (**2k**) and ${}^3\text{Hf}_2\text{O}_4$ (**2k**) show different behavior for water physisorption. The physisorption energy of ${}^3\text{Zr}_2\text{O}_4$ (**2k**) is ~4 kcal/mol more negative than that of ${}^1\text{Zr}_2\text{O}_4$ (**2k**). For M = Hf, the triplet physisorption energy is ~10 kcal/mol less negative than that of the singlet. For this isomer, the ${}^3\text{Zr}_2\text{O}_4$ – H_2O and ${}^1\text{Zr}_2\text{O}_4$ – H_2O bond distances are 2.29 and 2.42 Å, consistent with the physisorption energy difference. As the partial charges on Zr for the triplet and singlet of the complex are 1.34e and 1.67e, the Lewis acid–base bond distance between the water and the nanocluster is more important than the partial charge on the metal. For Hf_2O_4 (**2k**), the partial charges on Hf are 0.86e and 1.63e, and the Lewis acid–base bond distances are 2.28 and 2.37 Å for the triplet

Table 4. Mulliken Population Analysis for the Singlet and Triplet States for the Zirconium and Hafnium Oxides and Hydroxides at the B3LYP/aD Level

molecule ^a	Zr charge (S) ^c	Zr charge (T) ^d	Hf charge (S) ^c	Hf charge (T) ^d
ZrO ₂ (<i>C</i> _{2v} 1a) ^e	1.23	0.86	1.19	0.95
ZrO(OH) ₂ (1d)	1.51	1.32	1.42	1.02
Zr ₂ O ₄ (<i>C</i> _{2h} , 2a)	Zr(1): 1.37; Zr(2): 1.37	Zr(1): 1.28; Zr(2): 1.28	Hf(1): 1.39; Hf(2): 1.39	Hf(1,2): 1.08
Zr ₂ O ₄ (<i>C</i> _{2v} , 2h)	Zr(1): 1.37; Zr(2): 1.37	Zr(1): 1.27; Zr(2): 1.27	Hf(1): 1.40; Hf(2): 1.40	Hf(1,2): 1.08
Zr ₂ O ₄ (<i>C</i> _{3v} , 2k)	Zr(1): 1.54; Zr(3): 1.35	Zr(1): 1.40; Zr(3): 1.29	Hf(1): 1.88; Hf(3): 1.11	Hf(1): 1.96; Hf(3): 0.62
Zr ₂ O ₃ (OH) ₂ (2d)	Zr(8): 1.44; Zr(9): 1.23	Zr(8): 1.62; Zr(9): 1.21	Hf(8): 1.25; Hf(9): 1.79	Hf(8): 1.19; Hf(9): 1.57
Zr ₃ O ₆ (<i>C</i> _g , 3a) ^e	Zr(1): 1.59; Zr(4): 1.59; Zr(7): 1.05	Zr(1,4): 1.51; Zr(7): 0.55	Hf(1,4): 1.59; Hf(7): 1.24	Hf(1,4): 1.51; Hf(7): 0.55
Zr ₃ O ₆ (<i>C</i> ₁ , 4a)	Zr(1): 1.74; Zr(4): 1.10; Zr(7): 1.25	Zr(1): 1.89; Zr(4): 1.09; Zr(7): 0.90	Hf(1): 1.93; Hf(4): 1.23; Hf(7): 1.22	Hf(1): 2.04; Hf(4): 0.81; Hf(7): 1.26
Zr ₃ O ₆ (<i>C</i> ₂ , 5a)	Zr(1): 1.91; Zr(6,7): 1.16	Zr(1): 1.79; Zr(6,7): 1.11	Hf(1): 1.96; Hf(6,7): 1.17	Hf(1): 2.01; Hf(6,7): 1.00
Zr ₃ O ₆ (<i>C</i> _g , 6a)	Zr(1,2): 1.29; Zr(8): 1.25	Zr(1,2): 1.26; Zr(8): 1.18	Hf(1,2): 1.32; Hf(8): 1.28	Hf(1,2): 1.17; Hf(8): 1.26
Zr ₃ O ₅ (OH) ₂ (3d)	Zr(1,4): 1.39; Zr(7): 1.60	Zr(1): 1.19; Zr(4): 1.47; Zr(7): 1.44	Hf(1): 1.39; Hf(7): 1.47; Hf(7): 1.64	Hf(1): 1.19; Hf(4): 1.51; Hf(7): 1.41
Zr ₃ O ₅ (OH) ₂ (3g)	Zr(1): 1.46; Zr(4): 1.71; Zr(7): 1.02	Zr(1): 1.81; Zr(4): 1.49; Zr(7): 0.77	Hf(1): 1.36; Hf(4): 1.87; Hf(7): 1.22	Hf(1): 1.40; Hf(4): 1.93; Hf(7): 0.82
Zr ₃ O ₅ (OH) ₂ (3i)	Zr(1): 1.65; Zr(4): 1.61; Zr(7): 1.04	Zr(1): 1.74; Zr(4): 1.54; Zr(7): 0.85	Hf(1): 1.48; Hf(4): 1.87; Hf(7): 1.22	Hf(1): 1.58; Hf(4): 2.01; Hf(7): 0.75
Zr ₃ O ₅ (OH) ₂ (5d)	Zr(1): 1.57; Zr(6): 1.17; Zr(7): 1.56	Zr(1): 1.38; Zr(6): 1.16; Zr(7): 1.62	Hf(1): 1.71; Hf(6): 1.18; Hf(7): 1.49	Hf(1): 1.54; Hf(6): 1.10; Hf(7): 1.49
Zr ₃ O ₅ (OH) ₂ (5g)	Zr(1): 1.57; Zr(6): 1.29; Zr(7): 1.18	Zr(1): 1.73; Zr(6): 1.29; Zr(7): 1.12	Hf(1): 2.09; Hf(6): 1.28; Hf(7): 1.16	Hf(1): 1.99; Hf(6): 1.27; Hf(7): 0.98
Zr ₃ O ₅ (OH) ₂ (5i)	Zr(1): 1.74; Zr(6): 1.43; Zr(7): 1.27	Zr(1): 1.60; Zr(6): 1.44; Zr(7): 1.25	Hf(1): 1.73; Hf(6): 1.54; Hf(7): 1.26	Hf(1): 1.61; Hf(6): 1.51; Hf(7): 1.21
Zr ₃ O ₅ (OH) ₂ (5k)	Zr(1): 1.98; Zr(6): 1.27; Zr(7): 1.16	Zr(1): 1.84; Zr(6): 1.25; Zr(7): 1.14	Hf(1): 2.25; Hf(6): 1.27; Hf(7): 1.11	Hf(1): 2.17; Hf(6): 1.13; Hf(7): 1.01
Zr ₃ O ₅ (OH) ₂ (6d)	Zr(1): 1.36; Zr(2): 1.24; Zr(8): 1.48	Zr(1): 1.04; Zr(2): 1.28; Zr(8): 1.42	Hf(1): 1.22; Hf(2): 1.35; Hf(8): 1.90	Hf(1): 0.97; Hf(2): 1.32; Hf(8): 1.72
Zr ₃ O ₅ (OH) ₂ (6f)	Zr(1): 1.68; Zr(8,9): 1.19	Zr(1): 1.69; Zr(8): 0.94; Zr(9): 1.20	Hf(1): 1.61; Hf(8,9): 1.27	Hf(1): 1.55; Hf(8): 1.06; Hf(9): 1.23
Zr ₄ O ₈ (<i>C</i> _{2v} , 7a) ^e	Zr(1,8): 1.60; Zr(6,11): 0.86	Zr(1,8): 1.45; Zr(6): 0.87; Zr(11): 0.63	Hf(1,8): 1.33; Hf(6,11): 1.44	Hf(1,8): 1.50; Hf(6): 1.21; Hf(11): 0.88
Zr ₄ O ₈ (<i>C</i> _{2h} , 8a) ^e	Zr(1,8): 1.32; Zr(6,11): 1.46	Zr(1,8): 1.34; Zr(6,11): 1.04	Hf(1,8): 1.16; Hf(6,11): 1.87	Hf(1,8): 1.11; Hf(6,11): 1.39
Zr ₄ O ₈ (<i>C</i> _{2v} , 9a) ^e	Zr(2,3): 1.04; Zr(8,9): 1.45	Zr(1,8): 1.44; Zr(6,11): 0.73	Hf(2,3): 1.33; Hf(8,9): 1.41	Hf(2,3): 1.03; Hf(8,9): 1.45
Zr ₄ O ₇ (OH) ₂ (7d)	Zr(1): 1.31; Zr(6): 1.15; Zr(8): 1.35; Zr(11): 1.67	Zr(1): 1.33; Zr(6): 1.11; Zr(8): 1.03; Zr(11): 1.71	Hf(1): 1.28; Hf(6): 1.76; Hf(8): 1.32; Hf(11): 1.41	Hf(1): 1.07; Hf(6): 1.75; Hf(8): 1.34; Hf(11): 1.35
Zr ₄ O ₇ (OH) ₂ (7g)	Zr(1): 1.44; Zr(6): 1.19; Zr(8): 1.60; Zr(11): 1.17	Zr(1): 1.47; Zr(6): 1.00; Zr(8): 1.63; Zr(11): 1.10	Hf(1): 1.37; Hf(6): 1.47; Hf(8): 1.40; Hf(11): 1.42	Hf(1): 1.47; Hf(6): 1.00; Hf(8): 1.63; Hf(11): 1.10
Zr ₄ O ₇ (OH) ₂ (7i)	Zr(1): 1.33; Zr(6): 1.17; Zr(8): 1.83; Zr(11): 0.06	Zr(1): 1.42; Zr(6): 0.85; Zr(8): 1.92; Zr(11): 1.10	Hf(1): 1.20; Hf(6): 1.42; Hf(8): 1.81; Hf(11): 1.42	Hf(1): 1.46; Hf(6): 0.92; Hf(8): 1.75; Hf(11): 1.64
Zr ₄ O ₇ (OH) ₂ (8d)	Zr(1): 1.37; Zr(6): 1.28; Zr(8): 1.41; Zr(11): 1.73	Zr(1): 1.60; Zr(6): 1.25; Zr(8): 1.42; Zr(11): 1.23	Hf(1): 1.24; Hf(6): 1.66; Hf(8): 1.39; Hf(11): 1.90	Hf(1): 1.68; Hf(6): 1.82; Hf(8): 1.42; Hf(11): 0.88
Zr ₄ O ₇ (OH) ₂ (8g)	Zr(1): 1.46; Zr(6): 1.19; Zr(8): 1.59; Zr(11): 1.23	Zr(1): 1.38; Zr(6): 1.09; Zr(8): 1.84; Zr(11): 1.26	Hf(1): 1.37; Hf(6): 1.50; Hf(8): 1.39; Hf(11): 1.49	Hf(1): 1.73; Hf(6): 1.04; Hf(8): 1.27; Hf(11): 1.69
Zr ₄ O ₇ (OH) ₂ (8i)	Zr(1): 1.33; Zr(6, 11): 1.17; Zr(8): 1.83	Zr(1): 1.15; Zr(6, 11): 1.11; Zr(8): 1.80	Hf(1): 1.81; Hf(6, 11): 1.42; Hf(8): 1.20	Hf(1): 1.78; Hf(6): 1.58; Hf(8): 1.48; Hf(11): 0.93
Zr ₄ O ₇ (OH) ₂ (9d)	Zr(2): 1.38; Zr(3): 1.01; Zr(8): 1.28; Zr(9): 1.44	Zr(2): 1.42; Zr(3): 1.80; Zr(8): 1.30; Zr(9): 1.62	Hf(2): 1.33; Hf(3): 1.54; Hf(8): 1.37; Hf(9): 1.15	Hf(2): 1.06; Hf(3): 1.41; Hf(8): 1.77; Hf(9): 1.17
Zr ₄ O ₇ (OH) ₂ (9g)	Zr(2): 0.87; Zr(3): 1.04; Zr(8): 1.66; Zr(9): 1.64	Zr(2): 0.80; Zr(3): 0.91; Zr(8): 1.60; Zr(9): 1.76	Hf(2): 1.26; Hf(3): 1.41; Hf(8): 1.62; Hf(9): 1.42	Hf(2): 1.14; Hf(3): 1.26; Hf(8): 1.58; Hf(9): 1.64
Zr ₄ O ₇ (OH) ₂ (9i)	Zr(2): 0.92; Zr(3): 0.94; Zr(8): 1.40; Zr(9): 1.92	Zr(2): 0.82; Zr(3): 0.84; Zr(8): 1.65; Zr(9): 1.76	Hf(2): 1.23; Hf(3): 1.25; Hf(8): 1.43; Hf(9): 1.86	Hf(2): 1.08; Hf(3): 1.11; Hf(8): 1.95; Hf(9): 1.76

^aSee Figures 1–9 and Supporting Information for the molecular structures. ^bAtomic charge on Zr for the singlet states. See Supporting Information for the atomic labels. ^cAtomic charge on Zr for the triplet states. See Supporting Information for the atomic labels. ^dAt the BP86/aD level for the triplet states.

and the singlet, respectively. For this isomer, the less negative physisorption energy for the triplet as compared to the singlet is due to the much lower atomic charge on the metal.

The H₂O physisorption energies range from −20 to −45 kcal/mol for the isomers of ³M₃O₆. For isomers **3a** and **4a**, H₂O physisorption energies for the metal sites with an M=O bond are 4–9 kcal/mol more negative than those for the metal sites without an M=O bond. Isomer **5a** shows different

behaviors for its different binding sites. The reaction of H₂O binding to the metal site with an M=O bond is 2.6 kcal/mol less negative for M = Zr and 3.5 kcal/mol less negative for M = Hf than for the reaction of H₂O binding to the metal site without an M=O bond. The H₂O physisorption energies on ³Zr₃O₆ (**6a**) and ³Hf₃O₆ (**6a**) are −45.1 and −30.9 kcal/mol, respectively, comparable to the energies of the other isomers of ³M₃O₆. Compared to the energies of the singlet, the ³M₃O₆

isomers generally have more negative physisorption energies. However, there are exceptions for the isomers of ${}^3\text{Hf}_3\text{O}_6$, for example, the reaction $3\text{a} \rightarrow 3\text{d}$ and the reactions involving isomer 4a . The least negative adsorption energy, -17.1 kcal/mol , is calculated to be for $4\text{a} \rightarrow 3\text{d}$ for $\text{M} = \text{Hf}$, and the most negative adsorption energy, -47.2 kcal/mol , is found in the reaction $5\text{a} \rightarrow 5\text{d}$ for $\text{M} = \text{Zr}$.

The physisorption energies for the triplet states of the tetramers range from -15 to -45 kcal/mol and are in general more negative than those of the singlet state. For both ${}^3\text{Zr}_4\text{O}_8$ and ${}^3\text{Hf}_4\text{O}_8$, the most negative physisorption energy is calculated for $8\text{a} \rightarrow 8\text{e}$, and the least negative physisorption energy is for $9\text{a} \rightarrow 9\text{e}$. For the complex ${}^3\text{Zr}_4\text{O}_8\cdot\text{H}_2\text{O}$ (8e), the Lewis acid–base bond distance is 2.33 \AA , and the partial charge on Zr is 1.55e . In ${}^3\text{Zr}_4\text{O}_8\cdot\text{H}_2\text{O}$ (9e), the corresponding Lewis acid–base bond distance is 2.41 \AA , and the partial charge on Zr is 1.67e . For the complexes ${}^3\text{Hf}_4\text{O}_8\cdot\text{H}_2\text{O}$ (8e) and ${}^3\text{Hf}_4\text{O}_8\cdot\text{H}_2\text{O}$ (9e), the Lewis acid–base bond distances of ${}^3\text{Hf}_4\text{O}_8\cdot\text{H}_2\text{O}$ are 2.28 and 2.37 \AA , and the partial charges on Hf are 1.50 and 1.68e .

Overall, the physisorption energies for the triplet states are calculated to be -15 to -45 kcal/mol depending on the different structures and binding sites. The more negative physisorption energies, for example, $5\text{a} \rightarrow 5\text{b}$ and $8\text{a} \rightarrow 8\text{e}$, are due to the stabilization of the excited $\text{M}^*\text{--O}^*$ ($*$ indicates the unpaired electron) moiety. Similar to the singlet, the 2k isomers of ${}^3\text{M}_2\text{O}_4$ and the reaction $9\text{a} \rightarrow 9\text{e}$ are calculated to have less negative physisorption energies due to steric effects.

Chemisorption Energies of the $(\text{MO}_2)_n$ Nanoclusters

The first calculated hydrolysis reaction energies (dissociative chemisorption energies) of the $(\text{MO}_2)_n$ ($\text{M} = \text{Zr}, \text{Hf}, n = 1-4$) nanoclusters at 298 K are summarized in Tables 1 and 2. All of the calculated first hydrolysis reaction energies are exothermic as expected.

Singlet States. At the B3LYP/aT//B3LYP/aD level, the hydrolysis reaction energy for ZrO_2 reacting with one H_2O molecule to form ZrO(OH)_2 is calculated to be -75.5 kcal/mol . The same reaction energy for HfO_2 is calculated to be more negative than that for ZrO_2 by 10.1 kcal/mol . For the three isomers of the dimer, the chemisorption energies are calculated to be -70 to -80 kcal/mol for Zr_2O_4 and -80 to -90 kcal/mol for Hf_2O_4 . Thus, these energies for the dimers are comparable to that for the monomers.

For the different isomers of M_3O_6 , the chemisorption energies are calculated to be -30 to -80 kcal/mol for $\text{M} = \text{Zr}$ and -30 to -90 kcal/mol for $\text{M} = \text{Hf}$. The reaction forming two M--O bonds by H transfer to a terminal $=\text{O}$ after H_2O attaches to the metal with an $\text{M}=\text{O}$ bond is calculated to be the most exothermic for M_3O_6 ($3\text{a}, 4\text{a}, 5\text{a}$). For isomer 6a , the reaction for H transfer to the bridge $-\text{O}$ atom is calculated to be ca. -10 kcal/mol more exothermic than that of H transfer to a terminal $=\text{O}$ atom. A terminal $=\text{O}$ forms a bicoordinate $-\text{O}$ in the reaction of H transfer to a bridge $-\text{O}$ atom.

For the three isomers of M_4O_8 , the chemisorption energies are calculated to be -20 to -70 kcal/mol for $\text{M} = \text{Zr}$ and -20 to -80 kcal/mol for $\text{M} = \text{Hf}$. As in the reactions of the trimers, the reaction forming two M--OH bonds from an $\text{M}=\text{O}$ bond is calculated to be the most exothermic for isomers 7a and 8a . For isomer 9a , the reaction energy for $9\text{a} \rightarrow 9\text{i}$ to form two M--OH bonds by H transfer to a terminal $=\text{O}$ falls in the middle of those for the reactions $9\text{a} \rightarrow 9\text{d}$ and $9\text{a} \rightarrow 9\text{g}$. The $\text{M}=\text{O}$ bond in 9a is found not to be a real $\text{M}=\text{O}$ double bond

as the metal bonded with a terminal O atom has a stable tetracoordinate structure.

Triplet States. For ${}^3\text{MO}_2$, the chemisorption energies are calculated to be -59.0 and -61.7 kcal/mol for $\text{M} = \text{Zr}$ and $\text{M} = \text{Hf}$, respectively. These are ~ 10 and $\sim 20 \text{ kcal/mol}$ less negative than that for the singlet. For ${}^3\text{M}_2\text{O}_4$ ($2\text{a}, 2\text{h}, 2\text{k}$), the chemisorption energies are calculated to be ca. -85 kcal/mol for $\text{M} = \text{Zr}$ and ca. -90 kcal/mol for $\text{M} = \text{Hf}$. These are more negative than those for the singlet states. In contrast to the $\sim 10 \text{ kcal/mol}$ energy difference for the chemisorption energies for the three different singlet states, the same energy difference is only $\sim 2 \text{ kcal/mol}$ for the triplet states.

For ${}^3\text{Zr}_3\text{O}_6$, the chemisorption energies fall in the range -40 to -95 kcal/mol depending on the isomer and the specific reaction. The reaction energies for ${}^3\text{Hf}_3\text{O}_6$ are from -40 to -100 kcal/mol . As in the reactions of the singlets, the most exothermic reaction is calculated to be the reaction for forming two M--O bonds by H migration to a terminal $=\text{O}$ from H_2O attached to the metal with an $\text{M}=\text{O}$ bond, for example, the 3a , 4a , and 5a isomers of ${}^3\text{M}_3\text{O}_6$. The reaction energy for H transfer to a bridge $-\text{O}$ atom is slightly more negative than that for H transfer to a terminal $=\text{O}$ atom for ${}^3\text{Hf}_3\text{O}_6$ (6a). For ${}^3\text{Zr}_3\text{O}_6$ (6a), the reaction energy for H transfer to a bridge $-\text{O}$ atom is slightly less negative than that for H transfer to a terminal $=\text{O}$ atom. The reactions of the triplet isomers 7a , 8a , and 9a show the same trends as do the singlet states. The chemisorption energies for ${}^3\text{Zr}_4\text{O}_8$ fall into the range of -30 to -75 kcal/mol , and those energies for ${}^3\text{Hf}_4\text{O}_8$ fall in the range of -30 to -95 kcal/mol .

The first hydrolysis reaction energies for the $(\text{MO}_2)_n$ nanoclusters at 298 K are generally between -30 and -80 kcal/mol for the singlet state and -30 and -100 kcal/mol for the triplet state. The reactions of H_2O binding to the tetrahedral metal site in M_4O_8 (9a) have less negative chemisorption energies due to steric constraints. For each of the other isomers, the reaction forming two M--OH bonds from an $\text{M}=\text{O}$ bond shows more negative energies than other reactions because of the difference in the energies of the $\text{M}=\text{O}$ and M--O bond. The average bridge M--O bond energies are calculated to be 114 kcal/mol for $\text{M} = \text{Zr}$ and 116 kcal/mol for $\text{M} = \text{Hf}$, and the average terminal $\text{M}=\text{O}$ bond energies are calculated to be 164 kcal/mol for $\text{M} = \text{Zr}$ and 157 kcal/mol for $\text{M} = \text{Hf}$.⁴⁷ The reaction of H_2O with an $\text{M}=\text{O}$ bond leads to two M--OH bonds, and the M--O bonds can be considered to be single bonds. The reaction of H_2O binding to a bridge M--O bond leads to a terminal M--OH bond and a weaker bridge M--OH bond, a less exothermic process.

Lewis Acidities (Fluoride Affinities). The calculated Lewis acidities (fluoride affinities) of the different metal sites of the $(\text{MO}_2)_n$ ($\text{M} = \text{Zr}, \text{Hf}, n = 1-4$) nanoclusters at the B3LYP/aT//B3LYP/aD level are shown in Tables 1 and 2. (The fluoride affinity (FA) of A is the negative of the reaction enthalpy at 298 K of the reaction $\text{A} + \text{F}^- \rightarrow \text{AF}^-$.⁴⁸) We have previously calculated the FAs of the TiO_2 nanoclusters at the B3LYP/DZVP2 level.²⁴ The FA of ZrO_2 (1a) is quite high, $\sim 106 \text{ kcal/mol}$, but is less than the FA of both TiO_2 and HfO_2 (1a), ~ 119 and $\sim 113 \text{ kcal/mol}$.

The calculated FAs of the dimers are higher than that of MO_2 (1a). The binding sites for the F^- anion are the $\text{M}(\text{=O})(\text{--O})_2$ sites for M_2O_4 (2a) and M_2O_4 (2h) and the $\text{M}(\text{--O})_3$ site for M_2O_4 (2k). In addition, attaching the F^- anion to the $\text{M}(\text{=O})(\text{--O})_3$ site for M_2O_4 (2k) also leads to the conversion of a bridge M--O bond to a terminal $\text{M}=\text{O}$ bond. The FAs of

Zr_2O_4 (C_{2v} , **2a**) and Hf_2O_4 (C_{2h} , **2a**) are 17 and 10 kcal/mol lower than the FA of the Ti_2O_4 C_{2h} isomer (129 kcal/mol). The FAs of M_2O_4 for $M = Zr$ and Hf are also lower than that of Ti_2O_4 (C_{2v}) and Ti_2O_4 (C_{3v}) (125 and 138 kcal/mol, respectively).²⁴

For Zr_3O_6 (**3a**), the FA for the $Zr(-O)_3$ site is calculated to be much higher than that for the $Zr(=O)(-O)_3$ site. Attaching the F^- anion to Zr_3O_6 (**4a**) leads to the same $Zr_3O_6F^-$ product as that to Zr_3O_6 (**3a**); the FAs of those two sites are ~148 and ~114 kcal/mol. For Zr_3O_6 (**5a**), the FA for the $Zr(=O)(-O)_2$ site is calculated to be much higher than that for the $Zr(-O)_4$ site. When F^- is attached to a $Zr(=O)(-O)_2$ site of Zr_3O_6 (**6a**), one terminal $=O$ atom is converted to a tricoordinate $-O$ atom, and the product is the same as that for Zr_3O_6 (**3a**) leading to a high FA. When F^- is attached to the four different trimers for $M = Hf$, the reactions are similar to those for $M = Zr$, and the FAs for Hf_3O_6 are 6–12 kcal/mol higher than that for Zr_3O_6 for the same attachment site. The FAs for Zr_3O_6 and Hf_3O_6 range from ~90 to 167 kcal/mol and ~97 to ~179 kcal/mol, depending on the structure of the nanoclusters and the binding sites. From our previous work on the FAs for the different isomers of Ti_3O_6 ,²⁴ the reaction enthalpies range from ~97 to ~177 kcal/mol, falling in nearly the same range as the FAs for Hf_3O_6 . The spread of the FAs for the Ti_3O_6 isomer is somewhat larger than that of Zr_3O_6 .

For the tetramers, the FAs also depend on the structures and the metal sites. The FA of the $M(-O)_4$ site is higher than that of the $M(=O)(-O)_3$ site by 6–70 kcal/mol for M_4O_8 (**7a**, **8a**), and the FAs of the $M(-O)_4$ site are higher than that of the $M(=O)(-O)_3$ site by ~70 kcal/mol for M_4O_8 (**9a**). The fluoride affinities for Zr_4O_8 and Hf_4O_8 range from ~70 to ~140 kcal/mol and ~73 to 150 kcal/mol, respectively. In general, the FAs for Ti_4O_8 , Zr_4O_8 , and Hf_4O_8 lie in the same range.

Vibrational Frequencies. The calculated $M=O$ frequencies are given in Table 3. We provide these values for use in helping to analyze experimental data on such species when it becomes available. For the singlet states, the $Zr=O$ stretching frequencies are calculated to be 850–925 cm^{-1} , and the $Hf=O$ stretching frequencies are calculated to be approximately 20 cm^{-1} lower than those of $Zr=O$. The $Zr=O$ stretching frequency in $^1\text{ZrO(OH)}_2$ (**1d**) is calculated to be nearly equal to that of the largest one in $^1\text{ZrO}_2$ (**1a**), and the $Hf=O$ stretching frequency in $^1\text{HfO(OH)}_2$ (**1d**) falls between the two $Hf=O$ stretching frequencies in $^1\text{HfO}_2$ (**1a**). For the dimers, trimers, and tetramers, the terminal $M=O$ stretching frequencies of the hydroxides fall into the same range as those of the metal oxide nanoclusters. These results suggest that the addition of H_2O to one $M=O$ bond forming two $M-\text{OH}$ bonds has little effect on the geometry/frequencies of the remaining $M=O$ sites.

For the triplet states, for convenience, we refer to the terminal metal oxygen bonds as the double bonds, although some of the triplet state excitations occur in these bonds. Generally the longer $M=O$ distances result in decreases of up to 350 cm^{-1} for the $M=O$ stretching frequencies as compared to those in the singlet states. The $M=O$ frequencies in the triplet hydrolysis products can be similar to those in the singlet or substantially lower.

Triplet Atomic Spin Densities. The Mulliken atomic spin densities of the triplet states for the $(\text{MO}_2)_n$ ($M = \text{Zr}, \text{Hf}$, $n = 1\sim 4$) nanoclusters are given in the Supporting Information. The lowest-energy triplet excitation in MO_2 is in the $M=O$ bonds with nearly one spin on the metal atom and one-half spin

for each of the two O atoms. The lowest-triplet excitations in M_2O_4 (C_{2h} , **2a**), M_2O_4 (C_{2v} , **2h**), M_3O_6 (C_2 , **5a**), and M_3O_6 (C_s , **6a**) also involve the $M=O$ bonds. For the lowest triplet state of M_2O_4 (C_{3v} , **2k**), nearly one spin is on the terminal O atom, and one is on the M^{3+} center. The $M=O$ bond is not excited. For M_3O_6 (C_s , **3a**) and all the tetramers, the lowest-energy excitations occur on the metal site without an $M=O$ bond and the two terminal $=O$ atoms. For Zr_3O_6 (C_1 , **4a**), the excitation occurs in the $M=O$ bond. In contrast, the excitation involves the $Hf(4)=O$ bond for Hf_3O_6 (C_1 , **4a**).

For the hydroxides, the triplet excitations also involve the $M=O$ bonds in MO(OH)_2 (**1d**), $\text{M}_2\text{O}_3(\text{OH})_2$ (**2d**), $\text{M}_2\text{O}_3(\text{OH})_2$ (**3d**), $\text{M}_2\text{O}_3(\text{OH})_2$ (**5d**), $\text{M}_2\text{O}_3(\text{OH})_2$ (**5g**), $\text{M}_2\text{O}_3(\text{OH})_2$ (**5i**), $\text{M}_2\text{O}_3(\text{OH})_2$ (**5k**), $\text{M}_2\text{O}_3(\text{OH})_2$ (**6f**), and $\text{M}_4\text{O}_7(\text{OH})_2$ (**7d**). For $\text{M}_2\text{O}_3(\text{OH})_3$ (**3g**, **3i**) and $\text{M}_4\text{O}_7(\text{OH})_2$ (**7g**, **7i**, **8d**, **8g**, **9d**, **9g**), the excitations occur on one metal site without any $M=O$ bond and one terminal $=O$ atom. In $\text{Zr}_2\text{O}_3(\text{OH})_2$ (**6d**), the excitation lies in the $\text{Zr}(1)=\text{O}(6)$ atoms. The $Hf(1)=\text{O}(9)$ bonds are excited for $\text{Hf}_2\text{O}_3(\text{OH})_2$ (**6d**). There are differences between $\text{Zr}_4\text{O}_7(\text{OH})_2$ (**8i**) and $\text{Hf}_4\text{O}_7(\text{OH})_2$ (**8i**) as well as $\text{Zr}_4\text{O}_7(\text{OH})_2$ (**9i**) and $\text{Hf}_4\text{O}_7(\text{OH})_2$ (**9i**). The $\text{Zr}=O$ bond is excited in $\text{Zr}_4\text{O}_7(\text{OH})_2$ (**8i**), whereas the excitation in $\text{Hf}_4\text{O}_7(\text{OH})_2$ (**8i**) lies in the tetracoordinated $\text{Hf}(11)$ and the terminal $=O(9)$ atom. For $\text{Zr}_4\text{O}_7(\text{OH})_2$ (**9i**), the O atoms in two hydroxyl groups and the tetracoordinated $\text{Zr}(2)$ and $\text{Zr}(3)$ atoms are excited, whereas the O atoms in two hydroxyl groups are not excited in $\text{Hf}_4\text{O}_7(\text{OH})_2$ (**9i**). The two excited O atoms are replaced by one terminal $=O(10)$ atom in $\text{Hf}_4\text{O}_7(\text{OH})_2$ (**9i**).

DISCUSSION

The hydrolysis of the $(\text{MO}_2)_n$ ($M = \text{Zr}, \text{Hf}$, $n = 1\sim 4$) nanoclusters for both the singlet ground states and the lowest-energy triplet excited states is an exothermic process with low reaction barriers, less than 10 kcal/mol for most of the reactions studied. Thus, H_2O should readily react with the nanoclusters. For the first addition of water, as opposed to forming hydrogen bonds to the oxygen atoms in the cluster, the hydrolysis reaction begins with the exothermic physisorption of H_2O to the nanocluster to form a stable complex with a Lewis acid–base donor–acceptor bond. The adsorbed water decomposes by H transfer to form an $M-\text{OH}$ bond. For the trimers and tetramers, several different reaction types were studied. Water can bind to the site with $M=O$ or the site with $M-O$ followed by H transfer to either a terminal $=O$ atom or a bridge $-O$ atom.

The physisorption energies are dependent on the different adsorption sites and the cluster isomers. The more negative physisorption energies generally correlate with shorter $M-\text{H}_2\text{O}$ bond distances and higher Mulliken atomic charges at the adsorbed metal site. Steric effects can make the adsorption energies less positive, for example, **5a** → **5e** and **9a** → **9e**. Lower coordination numbers at a site can lead to more negative adsorption energies, for example, **5a** → **5b** and **9a** → **9d**. Restructuring of the cluster can also affect the adsorption energies, for example, **3a** → **3g**, in which a tricoordinate central O atom changes to a bicoordinate O atom. The location of the unpaired electrons in the triplet state can also play a role in the physisorption energies, generally leading to a more negative value if more energy is required to stabilize the excited $M^*-\text{O}^*$ moiety.

At 0 K, the chemisorption reaction energies for the first step are calculated to be exothermic, -20 to ca. -90 kcal/mol for the singlet ZrO_2 and HfO_2 clusters. For the triplets, the exothermic reaction energies of the ZrO_2 and HfO_2 clusters fall in a similar range of -20 to -100 kcal/mol. The second H_2O hydrolysis reactions for MO_2 and M_2O_4 are similar to the first H_2O hydrolysis reaction with reaction barriers less than 10 kcal/mol. The second steps are also exothermic for both $M = \text{Zr}$ and Hf with hydrolysis energies comparable to those for the first step. For the triplet reactions, the second step is much less exothermic than the first step, and the reaction barriers are still less than 10 kcal/mol. We predict that additional water can be added to the trimers and tetramers exothermically after the first hydrolysis step with low reaction barriers. For both singlets and triplets, the atomic charge of the metals in the nanoclusters to which water is bonded is lower than that in the corresponding hydroxide. For the singlet states, the chemisorption energies for ZrO_2 nanoclusters are generally more negative than those for the HfO_2 nanoclusters, but the energy differences are <12 kcal/mol between the two metals. The reactions to form two $\text{M}-\text{OH}$ bonds from an $\text{M}=\text{O}$ bond when water attaches to the metal bonded with the $=\text{O}$ atom are predicted to be more exothermic as compared to other reactions due to the difference in the bond energies of the $\text{M}=\text{O}$ and $\text{M}-\text{O}$ bonds. Isomer **9a** is an exception due to the very stable tetrahedral conformation of the $\text{M}=\text{O}$ site. The reactions of H_2O with nanoclusters are more exothermic when two $\text{M}-\text{OH}$ bonds are formed from an $\text{M}=\text{O}$ bond. Steric effects contribute significantly to the magnitude of the adsorption energies on different cluster structures.

Our present cluster calculations are relevant to water adsorption on the monoclinic and tetragonal ZrO_2 and HfO_2 surfaces.^{15,18,21} Both physisorption and chemisorption are observed on the crystal surface. Due to the more saturated coordination environment on monoclinic MO_2 surfaces than on tetragonal MO_2 surfaces,⁴⁹ the adsorption energy on the monoclinic surface is less negative than on the tetragonal surface as determined from both experiment¹⁵ and computation.²¹ For the singlet ground state MO_2 ($M = \text{Zr}, \text{Hf}$) nanoclusters, the H_2O physisorption energies are generally calculated to be -20 to -30 kcal/mol, and there is not much difference between M(III) and M(IV) sites or between $M = \text{Zr}$ and $M = \text{Hf}$. The range of physisorption energies increases to -15 to -48 kcal/mol for the triplet states. The experimentally measured water physisorption energy of -11.4 kcal/mol on ZrO_2 powder¹⁶ is less negative than our cluster values. Periodic DFT calculations¹⁹ report a physisorption energy of -12.4 kcal/mol on the tetragonal $\text{ZrO}_2(101)$ surface at 298 K, a smaller physisorption energy than our values for the clusters. Periodic plane-wave DFT calculations²¹ predicted a very low adsorption energy, -7 kcal/mol on the t- ZrO_2 tetragonal (101) surface at a coverage of 100%. However, calculations of lower coverages of 25% and 50% for the t- ZrO_2 (001), t- ZrO_2 (101), and m- ZrO_2 (001) surfaces yielded physisorption energies in the range of -20 to -24 kcal/mol, consistent with our cluster values. This is likely due to similarities in the metal coordination environments. The prediction of a physisorption energy of ca. -24 kcal/mol with a 50% coverage on a HfO_2 monoclinic (001) surface lies in the range of our results as well.²¹

The H_2O dissociative chemisorption on MO_2 nanoclusters to form a hydroxyl group instead of a hydrogen bond is consistent with previous studies on MO_2 surfaces.^{14,16,18,20,21,50,51} The

experimental chemisorption energies are between -31 to -45 kcal/mol and -26 to -41 kcal/mol on tetragonal ZrO_2 and HfO_2 surfaces,¹⁵ consistent with the calculated less exothermic reaction energies from the current study. The current lower range of the calculated chemisorption energies is consistent with existing computational studies of H_2O chemisorption energies, -20 to -50 kcal/mol on the monoclinic and tetragonal ZrO_2 surface^{18,20,21} and ca. -36 kcal/mol on the monoclinic HfO_2 surface.²¹ Due to structural similarities, the chemisorption energies on the tetragonal surfaces are nearly the same as the energies of chemisorption on a tetracoordinated metal site in one of our clusters that does not have an $\text{M}=\text{O}$ in the nanoclusters, for example, reactions **5a** \rightarrow **5g** and **7a** \rightarrow **7d**. The experimental chemisorption energies on the monoclinic surface are very close to that for the reaction of H_2O binding to the stable tetrahedral metal site, for example, reaction **9a** \rightarrow **9g**, because of a similar saturated coordination environment. We note that similar results were found when comparing the reactions of H_2O on TiO_2 clusters and surfaces.²⁴ Further work will be needed to improve the correlations between cluster and surface reactivity.

The reaction barriers for MO_2 nanoclusters for $M = \text{Zr}$ and $M = \text{Hf}$ are generally less than 10 kcal/mol, lower than those for $M = \text{Ti}$ for both the singlet and triplet states. The physisorption energies for both the singlet and triplet states for $M = \text{Zr}$ and $M = \text{Hf}$ fall into nearly the same range as that of the TiO_2 clusters. As found for the TiO_2 nanoclusters, there is little difference in the physisorption energies between M(III) and M(IV) sites. The exothermic chemisorption reactions for MO_2 nanoclusters $M = \text{Zr}$ and $M = \text{Hf}$ have reaction energies that are -10 to -20 kcal/mol more negative than those of the TiO_2 nanoclusters. The MO_2 nanoclusters for all three metals have similar hydrolysis properties. H_2O can readily react with these clusters as all of the reactions are exothermic with fairly low reaction barriers.

We have previously shown that the Lewis acidity (the fluoride affinity, FA) of a site correlates with the hydrolysis reaction energies of $(\text{TiO}_2)_n$ ($n = 1-4$) nanoclusters.²⁴ We find that the FAs show some correlation with the physisorption energies for the MO_2 clusters ($M = \text{Zr}, \text{Hf}$, Figure 10a). Those reactions, **2k** \rightarrow **2d**, **6a** \rightarrow **6d**, and **6a** \rightarrow **6f**, in which the addition of the F^- anion leads to a totally different cluster restructure, are not included in the plot. The metal site with the higher FA generally has the more negative physisorption energy, for example, the different M sites of the same cluster structure for M_3O_6 (**3a**), M_3O_6 (**5a**), M_4O_8 (**7a**), M_4O_8 (**8a**), and M_4O_8 (**9a**). The least negative physisorption energies for the $\text{M}(\equiv\text{O})(-\text{O})_3$ site of M_4O_8 (**9a**) are consistent with the lowest FAs for Zr and Hf . However, exceptions to this qualitative correlation can occur. For example, although the FA of ZrO_2 (**1a**) is calculated to be lower than that of Zr_2O_4 (**2a**) by ~ 7 kcal/mol, the physisorption energy of the former is 1 kcal/mol less negative than that of the latter. A similar inversion is found for the dimers. The FA of Zr_2O_4 (**2h**) is calculated to be higher than that of Zr_2O_4 (**2a**) by ~ 3 kcal/mol, but the physisorption energy of the former is less negative than the latter by ~ 0.2 kcal/mol. HfO_2 and Hf_2O_4 behave just like ZrO_2 and Zr_2O_4 in the correlation of Lewis acidity and physisorption energy. For M_3O_6 (**4a**), the higher FA on the $\text{M}(-\text{O})_3$ site corresponds to a less negative physisorption energy because the attachment of F^- results in the restructuring of M_3O_6 (**4a**), leading to a structure that is different from the one found when H_2O adsorbs. When F^- reacts at the $\text{M}(-\text{O})_3$ site, the

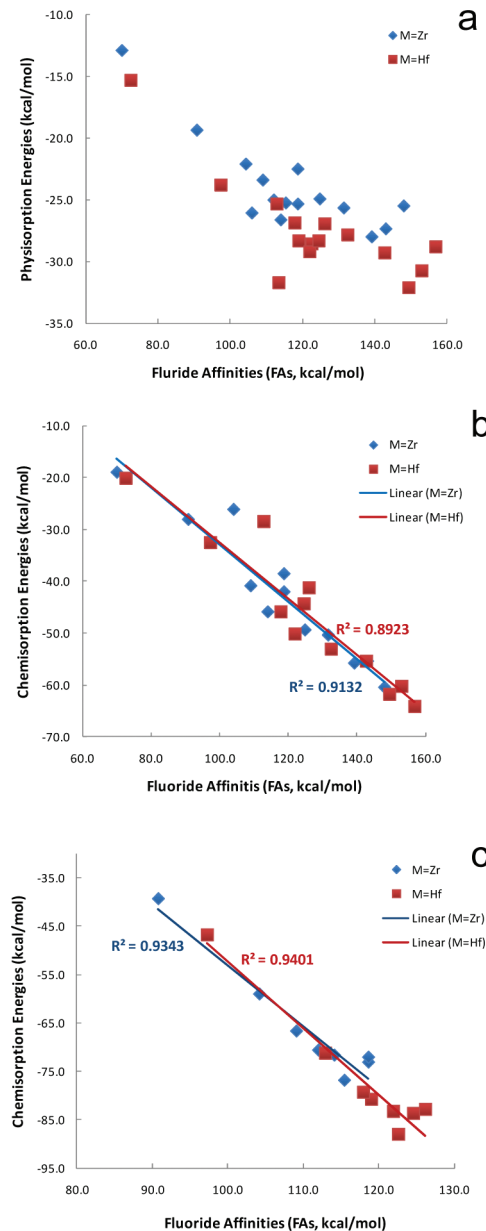


Figure 10. Plots of fluoride affinities vs reaction energies for $M = \text{Zr}$ and Hf . Those reactions in which the addition of the F^- anion leads to restructuring of the cluster ($2\text{k} \rightarrow 2\text{d}$, $6\text{a} \rightarrow 6\text{d}$, and $6\text{a} \rightarrow 6\text{f}$) are not included. (a) Physisorption energies. (b) Chemisorption energies for reactions of H transfer to an $-\text{O}$. (c) Chemisorption energies for the reactions of H transfer to a terminal $=\text{O}$. The reactions $1\text{a} \rightarrow 1\text{d}$ and $9\text{a} \rightarrow 9\text{i}$ are included plotted, as they have different O coordination types.

bicoordinate O atom in the ring is transformed to be a tricoordinate O atom. The restructuring of the bicoordinate O atom is not found for attachment of H_2O on the same site. The fact that a quantitative correlation between the FA and the physisorption energy does not exist could be due to the differences in the Lewis base strengths of F^- and H_2O with the former being a much stronger base. In addition, the ability of the cluster to stabilize the formal negative charge on the F^- may lead to different stabilizing interactions than with the H_2O , which does not have a charge to distribute into the cluster vacant orbitals. The donating lone pair orbital on the H_2O also has a specific orientation in contrast to F^- which could lead to

different interactions, and the H_2O may have larger steric interactions.

The correlation of chemisorption energy with the FA results in a more linear plot, as shown in Figure 10b for H transfer to a bridge $-\text{O}$ and in Figure 10c to a terminal $=\text{O}$. A site with a higher FA generally correlates with a more negative dissociative chemisorption energy for both H transfer reactions. The FAs do not really correlate with the reaction energy barriers, in part due to the very small barrier heights. In general, the adsorption energies and the reaction barriers depend on factors in addition to the Lewis acidity of the M site. These factors include the local structure of the M site and the O site to which the H atom is transferred, especially for the monomers and dimers.

Combining our previous work on TiO_2 nanoclusters²⁴ with the present work on ZrO_2 and HfO_2 nanoclusters, we can conclude that H_2O should readily decompose to generate two OH groups on Group 4 transition metal dioxide nanoclusters. The hydrolysis reactions of the nanoclusters are highly exothermic with very small activation energies. Therefore, little if any energy input is required for the hydrolysis steps. The overall H_2O splitting reaction to form H_2 and O_2 as given in reaction 1



is endothermic by ~ 116 kcal/mol. Approximately two 500 nm visible photons are needed just to overcome the endothermicity of reaction 1. The high exothermicities of the hydrolysis reactions if the Group 4 transition metal dioxide is used as photocatalyst and the reaction took place in the singlet state would require the input of substantially more energy to break the $\text{M}-\text{OH}$ bond to yield H_2 and O_2 . These reactions would be much easier on the excited state triplet surface. Further studies to quantify the energetics for the loss of H_2 and O_2 from these nanoclusters are underway.

CONCLUSIONS

Coupled cluster [CCSD(T)] theory and density functional theory (DFT) have been used to study the hydrolysis reactions of the singlet ground and first excited triplet states of the $(\text{MO}_2)_n$ ($\text{M} = \text{Zr}, \text{Hf}, n = 1-4$) nanoclusters. The first electronic excitations of any of these nanoclusters and the corresponding hydroxides involve the $\text{M}=\text{O}$ bond. The singlet-triplet gaps range from 720 to 350 nm so that many of the clusters can be excited by the solar visible spectrum, and the gaps depend on the size of the nanoclusters and their structure. The potential energy surfaces for the hydrolysis reactions of up to two H_2O with the monomers and dimers and one H_2O with the trimers and tetramers have been studied. The reaction is initiated by formation of a Lewis acid-base complex (physisorption) followed by H transfer to a terminal $=\text{O}$ or bridge $-\text{O}$ atom leading to the formation of the $\text{M}-\text{OH}$ bonds (dissociative chemisorption). This result is consistent with previous studies. The physisorption energies are calculated to be -20 to -30 kcal/mol for the singlet states and -15 to -48 kcal/mol for the triplet states. We did not find a large difference between adsorption at an M(III) or M(IV) site or between $\text{M} = \text{Zr}$ and $\text{M} = \text{Hf}$ sites. In general, H_2O prefers to adsorb on the M site with only a bridge $\text{M}-\text{O}$ bond for the singlet states with the exception of M_3O_6 (4a). The exception is due to the restructuring of the nanocluster on hydrolysis. Steric effects can lead to less negative physisorption energies, for example $9\text{a} \rightarrow 9\text{e}$. The singlet and triplet chemisorption energies for the first step range from -20 to

–100 kcal/mol and depend on different adsorption sites and different H transfer reactions. The reaction of H transfer to a terminal $=\text{O}$ bond is generally predicted to be more exothermic than that of H transfer to a bridge –O atom due to the substantial energy difference between the M=O and M–O bonds. The second steps for the hydrolysis of the monomers and dimers are also exothermic with the reaction energies comparable to the first step for the singlet and much less negative for the triplet. The reaction barriers are generally less than 10 kcal/mol with some of them nearly zero. Our results are consistent with previous work on the bulk surfaces, although we observe much more exothermic reactions in some cases.

■ ASSOCIATED CONTENT

Supporting Information

Complete references for numbers 37 and 45. Figures: atomic spin density for the triplet states of $(\text{MO}_2)_n$ ($\text{M} = \text{Zr}, \text{Hf}$, $n = 1–4$); molecular structures of the reaction of Hf_2O_4 , Hf_3O_6 , and Hf_4O_8 for Figures 2–9; Fluoride affinities for both ZrO_2 and HfO_2 isomers. Tables: CCSD(T) energies for the monomers; Physisorption energies at 0 K; Reaction barriers and enthalpies at 0 K; Enthalpies and Cartesian coordinates for all reactants, transition states, and products in Figures 1–9. This material is available free of charge via the Internet at <http://pubs.acs.org>.

■ AUTHOR INFORMATION

Notes

The authors declare no competing financial interest.

■ ACKNOWLEDGMENTS

This work was supported by the Chemical Sciences, Geosciences, and Biosciences Division, Office of Basic Energy Sciences, U.S. Department of Energy (DOE) under grant no. DE-FG02-03ER15481 (catalysis center program). D.A.D. also thanks the Robert Ramsay Chair Fund of The University of Alabama for support.

■ REFERENCES

- (1) Fujishima, A.; Honda, K. *Nature* **1972**, *238*, 37.
- (2) Fujishima, A.; Honda, K. *Chem. Soc. Jpn.* **1971**, *44*, 1148.
- (3) Sayama, K.; Arakawa, H. *J. Phys. Chem.* **1993**, *97*, 531.
- (4) Sayama, K.; Arakawa, H. *J. Photochem. Photobiol. A: Chem.* **1996**, *94*, 67.
- (5) Arakawa, H.; Sayama, K. *Catal. Surv. Jpn.* **2000**, *4*, 75.
- (6) Miller, J. E.; Allendorf, M. D.; Diver, R. B.; Evans, L. R.; Siegel, N. P.; Stuecker, J. N. *J. Mater. Sci.* **2008**, *43*, 4714.
- (7) Yin, L.; Niu, J.; Shen, Z.; Bao, Y.; Ding, S. *Mater. Lett.* **2011**, *65*, 3131.
- (8) Miyazakia, H.; Matsuia; Karuppuchamyb, H. S.; Uchizumia; Itoa, J. S.; Yoshiharaa, M. *Mater. Chem. Phys.* **2009**, *113*, 36.
- (9) Cardarelli, F. *Material Handbook*; Springer: London, 2000.
- (10) Tang, J.; Zhang, F.; Zoogman, P.; Steigerwald, M. L.; et al. *Adv. Funct. Mater.* **2005**, *15*, 1595.
- (11) Garvie, R. C. *J. Phys. Chem.* **1965**, *69*, 1238.
- (12) Payne, D. J. *Ph.D. Thesis*, University of Oxford: Oxford, U.K., 2008.
- (13) Holmes, H. F.; Fuller, E. L., Jr.; Gammage, R. B. *J. Phys. Chem.* **1972**, *76*, 1497.
- (14) Agron, P. A.; Fuller, E. L., Jr.; Holmes, H. F. *J. Colloid Interface Sci.* **1975**, *52*, 553.
- (15) Ushakov, S. V.; Navrotsky, A. *Appl. Phys. Lett.* **2005**, *87*, 164103.
- (16) Raz, S.; Sasaki, K.; Maier, J.; Riess, I. *Solid State Ionics* **2001**, *143*, 181.
- (17) Brunauer, S.; Emmett, P. H.; Teller, E. *J. Am. Chem. Soc.* **1938**, *60*, 309.
- (18) Añez, R.; Sierraalta, A.; Martorell, G. *J. Mol. Struct. Theochem.* **2009**, *900*, 59.
- (19) Hofmann, A.; Sauer, J. *J. Phys. Chem. B* **2004**, *108*, 14652.
- (20) Ignatchenko, A.; Nealon, D. G.; Dushane, R.; Humphries, K. *J. Mol. Catal. A: Chem.* **2006**, *256*, 57.
- (21) Iskandarovaa, I. M.; Knizhnikaa, A. A.; Rykovaa, E. A.; Bagatur'yantsa, A. A.; Potapkina, B. V.; Korkin, A. A. *Microelectron. Eng.* **2003**, *69*, 587.
- (22) (a) Li, S.; Hennigan, J. M.; Dixon, D. A.; Peterson, K. A. *J. Phys. Chem. A* **2009**, *113*, 7861. (b) Li, S.; Dixon, A. D. *J. Phys. Chem. A* **2010**, *114*, 2665.
- (23) Li, S.; Dixon, D. A. *J. Phys. Chem. A* **2008**, *112*, 6646.
- (24) Wang, T.; Fang, Z.; Gist, N. W.; Li, S.; Dixon, D. A.; Gole, J. L. *J. Phys. Chem. C* **2011**, *115*, 9344.
- (25) Parr, R. G.; Yang, W. *Density-Functional Theory of Atoms and Molecules*; Oxford University Press: New York, 1989.
- (26) Becke, A. D. *J. Chem. Phys.* **1993**, *98*, 5648.
- (27) Lee, C.; Yang, W.; Parr, R. G. *Phys. Rev. B* **1988**, *37*, 785.
- (28) Purvis, G. D., III; Bartlett, R. J. *J. Chem. Phys.* **1982**, *76*, 1910.
- (29) Raghavachari, K.; Trucks, G. W.; Pople, J. A.; Head-Gordon, M. *Chem. Phys. Lett.* **1989**, *157*, 479.
- (30) Watts, J. D.; Gauss, J.; Bartlett, R. J. *J. Chem. Phys.* **1993**, *98*, 8718.
- (31) Kendall, R. A.; Dunning, T. H., Jr.; Harrison, R. J. *J. Chem. Phys.* **1994**, *96*, 6796.
- (32) (a) Peterson, K. A.; Figgen, D.; Dolg, M.; Stoll, H. *J. Chem. Phys.* **2007**, *126*, 124101. (b) Figgen, D.; Peterson, K. A.; Dolg, M.; Stoll, H. *J. Chem. Phys.* **2009**, *130*, 164108.
- (33) McQuarrie, D. A. *Statistical Mechanics*; University Science Books: Sausalito, CA, 2000.
- (34) Becke, A. D. *Phys. Rev. A* **1988**, *38*, 3098.
- (35) Perdew, J. P. *Phys. Rev. B* **1986**, *33*, 8822.
- (36) Peng, C.; Schlegel, H. B. *Isr. J. Chem.* **1993**, *33*, 449.
- (37) Frisch, M. J.; Trucks, G. W.; Schlegel, H. B.; Scuseria, G. E.; Robb, M. A.; Cheeseman, J. R.; Scalmani, G.; Barone, V.; Mennucci, B.; Petersson, G. A.; et al., *Gaussian 09*, revision B.1; Gaussian, Inc., Wallingford CT, 2009.
- (38) Peterson, K. A.; Woon, D. E.; Dunning, T. H., Jr. *J. Chem. Phys.* **1994**, *100*, 7410.
- (39) (a) Peterson, K. A.; Figgen, D.; Dolg, M.; Stoll, H. *J. Chem. Phys.* **2007**, *126*, 124101. (b) Figgen, D.; Peterson, K. A.; Dolg, M.; Stoll, H. *J. Chem. Phys.* **2009**, *130*, 164108.
- (40) Li, S.; Hennigan, J. M.; Dixon, D. A.; Peterson, K. A. *J. Phys. Chem. A* **2009**, *113*, 7861.
- (41) (a) Douglas, M.; Kroll, N. M. *Ann. Phys.* **1974**, *82*, 89. (b) Hess, B. A. *Phys. Rev. A* **1985**, *32*, 756. (c) Hess, B. A. *Phys. Rev. A* **1986**, *33*, 3742.
- (42) (a) Peterson, K. A.; Figgen, D.; Dolg, M.; Stoll, H. *J. Chem. Phys.* **2007**, *126*, 124101. (b) Figgen, D.; Peterson, K. A.; Dolg, M.; Stoll, H. *J. Chem. Phys.* **2009**, *130*, 164108.
- (43) De Jong, W. A.; Harrison, R. J.; Dixon, D. A. *J. Chem. Phys.* **2001**, *114*, 48.
- (44) Balabanov, N. B.; Peterson, K. A. *J. Chem. Phys.* **2005**, *123*, 64107.
- (45) Werner, H.-J.; Knowles, P. J.; Manby, F. R.; Schütz, M.; Celani, P.; Knizia, G.; Korona, T.; Lindh, R.; Mitrushenkov, A.; Rauhut, G.; et al. *MOLPRO*, version 2010.1, a package of *ab initio* programs, see <http://www.molpro.net>.
- (46) AMPAC 9; Semichem, Inc.: 12456 W 62nd Terrace - Suite D, Shawnee, KS 66216, 1992–2008.
- (47) Li, S.; Hennigan, J. M.; Dixon, D. A.; Peterson, K. A. *J. Phys. Chem. A* **2009**, *113*, 7861.
- (48) (a) Christe, K. O.; Dixon, D. A.; McLemore, W. W.; Sheehy, J.; Boatz, J. A. *J. Fluorine Chem.* **2000**, *101*, 151. (b) *Chem. Eng. News*, **2003**, Mar. 3, 48–49.
- (49) Luo, X.; Zhou, W.; Ushakov, S. V.; Navrotsky, A.; Demkov, A. *A. Phys. Rev. B* **2009**, *80*, 134119.

- (50) Radha, A. V.; Bomati, M. O.; Ushakov, S. V.; Navrotsky, A.; Tartaj, P. *J. Am. Ceram. Soc.* **2009**, *92*, 133–140.
(51) Driemeier1, C.; Gusev, E. P.; Baumvol, I. J. R. *Appl. Phys. Lett.* **2006**, *88*, 201901.